CHALMERS

Study of wall thickness and its impact on microstructure on 316L manufactured with Direct Metal Laser Sintering

Bachelor thesis in Mechanical Engineering

JOHANNA TIMHAGEN
DANIEL NALUM

Bachelor thesis number: 173/2017

Department of Materials and Manufacturing Technology
CHALMERS UNIVERSITY OF TECHNOLOGY
Gothenburg, Sweden 2017

Study of wall thickness and its impact on microstructure on 316L manufactured with Direct Metal Laser Sintering
Bachelor thesis number: 173/2017
Johanna Timhagen, Daniel Nalum

Supervisor: Alexander Leicht
Examiner: Lars Nyborg

Chalmers University of Technology
Department of Materials and Manufacturing Technology
SE-412 96 Gothenburg, Sweden 2017

PREAMBLE

The bachelor thesis "Study of wall thickness and its impact on microstructure on 316L, manufactured with direct selective laser melting", are written by Johanna Timhagen and Daniel Nalum, and marks the end of our education, Mechanical engineering 180 hp. This corresponds to three years of full time studies at bachelor level. The thesis has been executed in about 20 weeks, beginning in January 2017 and ending in June 2017, and corresponds to 15 hp.

The study has been completed at the Department of Materials and Manufacturing Technology at Chalmers University of Technology. The thesis has been part of a larger study conducted at the department on how the DMLS technique impacts the microstructure of components fabricated in stainless steel 316L.

We want to thank the staff at Volvo Materials Technology, who has contributed with their knowledge as well as their equipment, such as microscopes, etc. We also want to thank our examiner at Chalmers University of Technology, Lars Nyborg, who came up with the idea of the project and our mentor Alexander Leicht, who we have worked closely with and has been a great support throughout the entire project.

ABSTRACT

The aim off this thesis was to theoretically and experimentally study how the microstructure of additively manufactured 316L (stainless steel) components is affected by different wall thicknesses. In addition, hardness and porosity are analyzed with a perspective of wall thickness. In this study 9 different thicknesses, ranging from 0,2 mm up to 3 mm, were selected. The structure was cut in a way so that the middle part of each wall could be observed to exclude edge defects. The samples were analyzed with a Leica DMi8 microscope was pictures was taken and stitched for a porosity analyses. The analysis showed a low number of pores which were overall small. A Vickers hardness measurement was done in a Struers DuraScan to observe if the wall thickness affected the micro hardness of the material. No significant correlation was found and the hardness does not seem to be affected by either wall thickness, position of cross section or edge effects. Electrochemical etching was performed to reveal the microstructure of the material. Melt pools, solidification structure and sub-grains emerged during this process. A more detailed investigation was conducted and the solidification structure of the material was observed. The result shows a microstructure containing large areas of sub-grains with the same orientation, creating a columnar solidification structure which follows the building direction. The results indicate that the orientation of the grains is affected by the wall thickness.

Keywords: AM, SLM, DMLS, 316L, EOS, wall thickness, microstructure, sub-grains, solidification structure, hardness testing, porosity testing.

Table of Contents

DESIGNATIONS

AM	Additive Manufacturing
DMLS	Direct Metal Laser Sintring
SEM	Scanning Electron Microscope
EBSD	Electron BackScatter Diffraction
SD	Standard Deviation
SS	Stainless Steel
BD	Building Direction

1. INTRODUCTION

Additive manufacturing (AM) is under development and is now seen as a realistic method for fabrication of parts in many areas. The method introduces the possibility for new products and applications, largely due to a greater design freedom. Unlike conventional manufacturing methods, AM adds material instead of removing material, consequently the need for tools etc. are no longer needed. Furthermore, since AM is a near-net-shaped process a reduction of post processing of AM components can generally be achieved. Besides, the batch sizes do not need a certain amount of components to be profitable, since AM makes it possible to make unique components without a larger cost. The obvious advantages have contributed to a large amount of research and development and are therefore a technology that has taken a great leap since the early 2000s.

1.1 Background

The research on additive manufacturing is interesting, inspiring and a future area when it comes to materials science, manufacturing technology and mechanical engineering. Chalmers University of Technology in Gothenburg, Sweden, is preforming research on additive manufacturing of metals. This study is involved in the research that is conducted at the Department of Materials and Manufacturing Technology.

The development of additive manufacturing has been ongoing for a few decades and many of the early problems, like process parameters, building techniques and methods have now been solved. The research nowadays is focused on characterization of mechanical properties and microstructure for AM fabricated materials.

Additive manufacturing includes several rapidly developing technologies. Among these, Direct Metal Laser Sintering (DMLS), is the dominant powder bed based method for manufacturing metal components. For stainless steel components, the technology has demonstrated great design freedom and has enabled production of high performance products with a high degree of complexity with comparable properties to conventional methods. The process is well established to produce stainless steel products. To optimize the weight further, the wall thickness must be reduced, which requires high demands on material properties and therefore also the material structure.

1.2 Aim

The aim with this investigation is to theoretically and experimentally study how the microstructure of additively manufactured components is affected by different wall thicknesses, in particular thin walls. The results could be used to create design rules for lightweight production in e.g. stainless steel.

1.3 Limitations

The study will not take different techniques or different machines abilities into consideration when evaluating the final components, only components produced by means of EOS M290 will be included. Components will be made using stainless steel 316L metal powder from EOS and all components will be produced using standard process parameters.

Extensive mechanical testing (tensile tests, creep tests, fatigue, etc.) are important when evaluating the material, but this study is limited to examination of porosity, hardness testing and microstructure. The components will be investigated in an as-built-condition, and therefore no post heat treatment will be performed.

1.4 Research questions

- Does the wall thickness affect the microstructure of a 316L components manufactured by the DMLS technique? If so, what kind of effects can be seen and which wall thickness is needed to prevent these effects?
- Does wall thickness affect the hardness of the DMLS manufactured 316L material?
- Can differences in hardness been observed when comparing different areas of the samples?
- Does the wall thickness affect the amount and/or size of pores in the structure?

2. LITERATURE SURVEY

This chapter will cover the theoretical parts needed for this study. It will both focus on basics of the technology itself, together with more profound theory about material and methods of testing.

2.1 Basics of additive manufacturing

Additive manufacturing (AM), also known as 3D-printing, is a way to manufacture different products in a large range of materials [1]. The technology is based on a layer-by-layer principle where the material is added as liquids, powder, molten or as sheets. The way of adding the material is often linked to the type of material used in the process. The process was originally developed for polymeric materials, paper and waxes but is today also used for other materials such as ceramics, composites and metals. Today AM can be used for fabrication of fully functional parts by several different techniques and materials.

The AM process starts by creating a 3D-model, where the product is modeled. The model is converted into a stl-file (STereoLithography), which will only contain information about the surface geometry. The stl-file need to be manipulated in another software to slice the component and thereby creating the layers, which then will be used for building the component in a layer-by-layer manner [2]. The sliced model is loaded into the machine and the process is set. The process can start when all processing parameters are established. When the build is finalized depending on process excess material needs to be removed and support structures need to be detached by machining.

2.2 Technologies

Additive manufacturing can be divided in to three different categories, “powder bed systems”, “powder feed systems” and “wire feed systems” [3]. For powder bed systems, powder is layered on a working area by raking thin layers of powder. An energy source then melts a specific area, defined by the CAD-model, of the powder bed. When the layer is done, the work area is lowered down to make place for another layer of powder upon the plate, and then the process continues until the build is completed. Some advantages with this system are high dimensional control and high-resolution ability. However, most of the systems today cannot deliver large products meaning that the total volume is limited to 0.03 m^3, at the same time as the building itself is time consuming.

Powder feed systems on the other hand, blows powder over the work area through a nozzle and uses laser to melt the powder in that specific area to build the component. The system allows both the building plate and the nozzle to move to add new powder. The powder feed systems often allow larger components, up to 1.2 m^3, which makes it suitable for renovating and reconditioning of used components [3].

The wire feed system is similar to the powder feed system, but is instead feeding the material as a stock wire. The process can be compared with conventional MIG/MAG welding. The main advantage of this system is the high deposition rate, where large products can be manufactured in high speed. The disadvantages on the other hand, are that products created in this process need more post processing [3].

2.2.1 Direct Metal Laser Sintering (DMLS)

DMLS (also known as selective laser melting (SLM), selective laser sintering (SLS) and laser melting (LM)) is a powder bed system technology [4]. The common name laser sintering (LS)

frames the different acronyms even if nowadays the powder is fully melted. For this process, each layer of powder is ranging from 20-100 μm in thickness. The building parameters, such as laser energy, scanning speed, hatch spacing and layer thickness are used for ensuring fabrication of high quality parts with high density. To accomplish this, the melt pool need to be fused together, both on each side, but also with the previous layer underneath. The parameters are therefore carefully set to match both productivity and quality. Since the process is conducted at high temperatures, the process needs to be protected from oxidation. To ensure a "clean" process, the building chamber is filled with argon or nitrogen gas to create an inert atmosphere. To reduce thermal stress, the building plate is generally preheated.

2.3 Microstructure in DMLS manufactured components

There are two primarily features that has a significant impact on the microstructure [4]. Firstly, the layer on layer method that the DMLS processes use result in a repeated phase transformation between solid and liquid due to re-melting of the layers beneath. Secondly, the process is characterized by its fast cooling rates. The fast cooling rates result in a solidification process that is not in equilibrium [5]. Depending on the cooling rate the size of the sub-grains will differ. The cooling rate for the AM process is very high, which makes very small sub-grains expected, since they do not have the time to increase in size. However, the re-melting enables the grains to grow over several layers, making the grains large. The microstructure of AM parts is therefore in general very complex due to the complex thermal history.

The grains grow perpendicular to the building plate and in the direction of the temperature gradient, which could make the anisotropy of the microstructure affect the mechanical properties. The building direction has been shown in some cases to be the weakest for 316L [5]. However, there has not been any clear explanation for this.

2.3.1 Cellular-dendritic structure

In DMSL manufactured components, a cellular-dendritic structure is known to occur. The most important variables for the microstructure to either develop a cellular or a dendritic structure seems to be the solidification velocity and the temperature gradient, see in *Figure 2.1.* When the velocity increase and the solidification time becomes slower, especially for a single phase alloys [6], a transition from cellular to dendritic structure takes place. The dendritic structure will then develop primary, secondary and sometimes even tertiary branches [7]. These branches will grow in the easiest and least energy consuming direction, which results in the dendritic structure to take a tree-like shape.

Cellular structure on the other hand develops mostly when the solidification time is short [8]. This makes the cellular structure look needle like. The cellular-dendritic structure has no secondary branches and occurs in the transition stage between cellular and dendritic. It will look similar to the cellular structure and is normally found in DMLS manufactured materials, especially 316L [9].

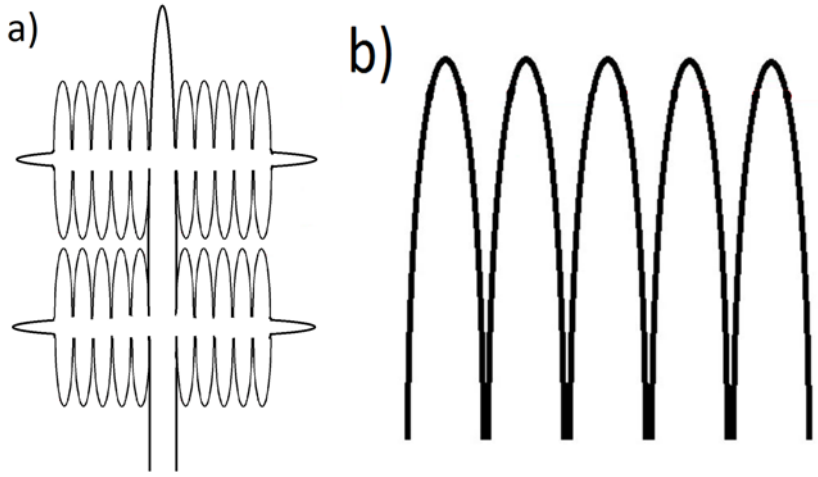

Figure 2.1: Sub-grains. a) Dendritic struture. b) Cellular structure.

2.4 Stainless steel

Austenitic stainless steel is a common type of stainless steel (SS) that in general has a high corrosion resistance, outstanding cryogenic properties and good high-temperature strength [8]. The varying temperature abilities come from their austenitic microstructure that is very tough and ductile. Austenitic stainless steel in the 300-series is chromium-nickel alloys.

An approach to divide austenitic SS in to groups can be done in the following way: Lean austenitic SS, High-temperature austenitic SS and Enhanced corrosion-resistant austenitic SS. While the group names are rather telling their abilities, more explanatory Lean austenitic SS consist of less than 20% Cr and 14% Ni. The SS of this group are generally used for their high strength or high formability. High-temperature austenitic SS on the other hand, are enhanced through silicon, and are used for their high-temperature oxidation resistance.

Finally, enhanced corrosion-resistant austenitic SS, has improved corrosion resistance, owing to the use of chromium, molybdenum, nickel and nitrogen. Furthermore, to enhance resistance to more specific corrosive environments, silicon and copper are added. 316L belong to this group.

2.4.1 Stainless Steel 316L

The 316L is an austenitic stainless steel, in particular a chromium-nickel alloy. When the chromium and chromium equivalents content increase, nickel and nickel equivalents need to increase as well. It is important to have matching amounts of chromium and nickel to maintain the austenitic microstructure. The chemical composition of the 316L powder used in this study are in accordance with EOS material data sheet shown in *Table 2.1*[10].

Table 2.1: Elements of Stainless Steel 316L, contents in wt%.

Fe	Cr	Ni	Mo	C	Mn
Balance	17.00-19.00	13.00-15.00	2.25-3.0	≤0.030	≤2.00
Cu	P	S	Si	N	
≤0.50	≤0.025	≤0.010	≤0.75	≤0.10	

Each of the elements has a purpose, which is the following [8]:

Chromium (Cr) - gives the basic corrosion resistance, the corrosion resistance is improved by increasing the Cr content. It also promotes a ferritic microstructure.
Nickel (Ni) - promotes an austenitic microstructure, which increases ductility and toughness. The Ni reduces the corrosion rate and it is therefore beneficial in corrosive environments.
Molybdenum (Mo) - added to increase resistance to both uniform and localized corrosion. The mechanical strength is increased slightly by the Mo, but the element strongly promotes a ferritic microstructure.
Carbon (C) - strongly enhances austenitic formation and increases mechanical strength. The C will make the Cr diffuse and create carbides, which means there are not enough free Cr left to generate the protective oxide layer.
Manganese (Mn) - enables a higher level of nitrogen since manganese increase nitrogen's solubility. At low temperatures, Mn acts as an austenitic stabilizer, however in high temperatures at acts as a ferritic stabilizer instead.
Nitrogen (N) - strong austenitic former that increases mechanical strength. It also increases resistance to localized corrosion, especially combined with manganese.
Sulphur (S) - increases machinability and slightly reduces corrosion resistance as well as ductility, weldability and formability.

The various types of phases present in stainless steel can be visualized in a Scheaffler DeLong diagram, which was developed for this very purpose and can be seen in *Figure 2.2*. The diagram is used for predicting the as-solidified condition of the stainless steel, and uses two equations, one for chromium equivalents and one for nickel equivalents, to allow this.

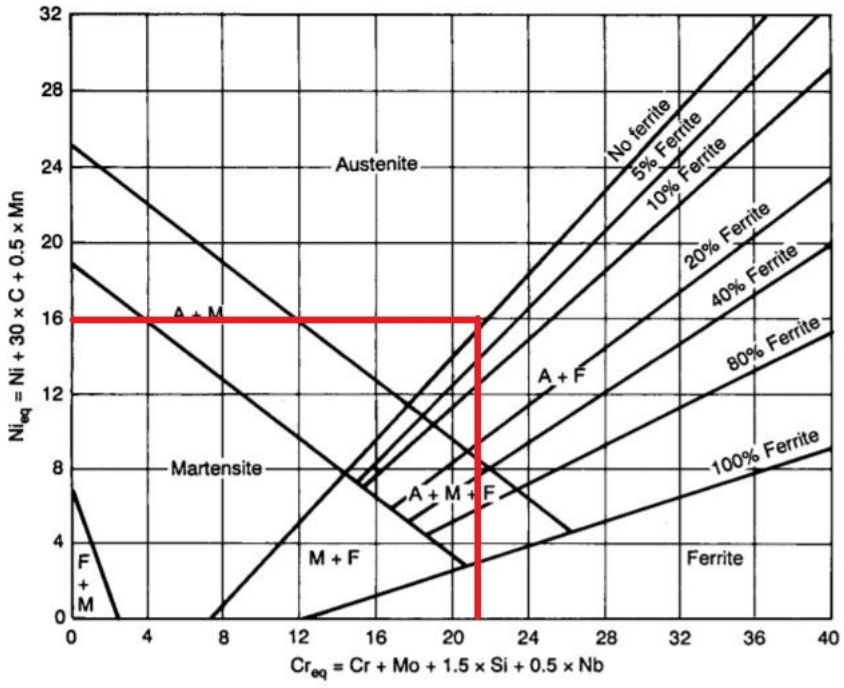

Figure 2.2: Scheaffler DeLong diagram [8] were the red line show 316L

Equation for Chromium equivalents:

$$Cr_{eq} = Cr + Mo + 1.5 * Si + 0.5 * Nb \quad (1)$$

Equation for Nickel equivalents:

$$Cr_{eq} = Ni + 30 * C + 0.5 * Mn \quad (2)$$

Using these two equations for an average value of the components, gives a chromium equivalent level of 21.7% and a nickel equivalent level of 16%. In *Figure 2.2*, each of these levels are shown by two lines that meet in the austenitic field of the diagram.

2.4.2 Gas atomized 316L powder

Wanted characteristics for powder used in AM are high packing efficiency and the ability to make even homogeneously distributed layers. The layer should be flat and thin. These types of powders are usually pre-alloyed gas-atomized with a high degree of sphericity and roundness with a smooth surface [11]. The powder used in this study is EOS Stainless Steel 316L and has particles in the size between 20-53 μm.

2.5 Porosity

Porosity in DMLS manufactured parts can be categorized into two types, gas-induced porosity and process-induced porosity. Gas-induced pores tend to have a spherical shape of size less than 5 μm [12]. The gas pores can be created due to two reasons. Firstly, gas can be entrapped in the metal particle, during the gas atomization of the feedstock material. Secondly, gas from the build chamber can be entrapped into the melt/melt pool during the build. Since argon is used for both the powder production but also for the build it is possible that either of these reasons makes gas pores become part of the finished components.

Process-induced porosity on the other hand, tend to be non-spherical. This porosity is formed due to two reasons, either a lack of energy or an excessive amount of energy during the process. A lack of energy will fail to make the powdered layers to fuse properly, therefore creating uneven pores. Excessive energy will on the contrary result in spatter ejection [12]. In general, it can be expected from 316L components manufactured by DMLS to have a high densification level (>99%) and low average porosity content (~0.82%). The same samples showed porosity unevenly distributed through the samples.

2.6 Hardness testing

Hardness is a term that can be specified as the ability within a body to counteract penetration of another body with a certain resistance [13]. Higher resistance results in higher hardness. The hardness of a body is also related to velocity; thus, a soft lead bullet can leave a scratch on a hardened steel plate if the velocity of the bullet is high.

Vickers is a static hardness test where the hardness is tested under an applied test force. The indenter is a diamond, shaped as an equilateral pyramid with a square base with a 136-degree angle in between opposite faces, see *Figure 2.3*. The advantage of the equilateral pyramid is that the law of proportional resistance can be applied, and results can be compared regardless of test force. The result of the test is defined as a quotient between force (F) and penetrated surface area (A) of the remaining indentation. The surface area (A) is calculated with the two diagonals d1 & d2.

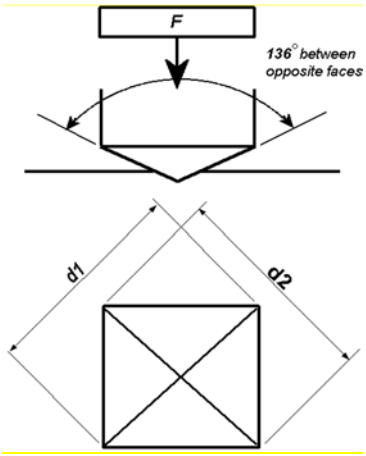

Figure 2.3: At top: Vickers indenter, equilateral squared based diamond pyramid. At bottom: Vickers indentation with diagonal 1 and diagonal 2 showed.

When applying the force in a hardness testing machine, the force is given as kgf (kilogram force). This gives that HV1 (Hardness Vickers 1 kgf) is loaded with a total of 9.807 N. The range of loads varies from 0.01 kgf to 1 kgf (micro Vickers) and from 5 kgf to 100 kgf (macro Vickers).

Vickers is an ISO 6507 certified standard of hardness testing, giving a few rules to follow. Applied load should, due to the certificate, result in an indentation with a diagonal of 20 µm up to 1.4 mm. A sample surface needs to be at least 2.5 x 2.5 times the expected diagonal and at least 1.5 times the diagonal thick. Indentations need to have at least 3 times the diagonal as center distance from one another to not affect the results.
The hardness is calculated by:

$$HV = \frac{0.102 * F}{A} \tag{3}$$

where

$$A = \frac{d^2}{2 * \sin 68} \tag{4}$$

and

$$d = \frac{(d_1 + d_2)}{2} \tag{5}$$

hence →

$$HV = \frac{0.102 * 1.854 * F}{d^2} \tag{6}$$

2.7 Surface roughness

Surface roughness is measured in different ways, where R_a, R_q and R_z are the most common measures, and can be described as a spread of surface peaks and troughs. The measures describe the surface of the material but differ a bit when assessing the results. The R_a, classified as the arithmetic average height parameter, is normally used when talking about fatigue strength. The parameter is an average deviation from the mean line over a specific length, described in equation 7 [14].

$$R_a = \frac{1}{l}\int_0^l |y(x)|dx \tag{7}$$

The R_q, on the other hand, is the mean square root roughness, which is described as the standard deviation of the distribution of surface heights [14]. This value is more sensitive to deviation than R_a and is described in equation 8.

$$R_q = \sqrt{\frac{1}{l}\int_0^l \{y(x)\}^2 dx} \tag{8}$$

The R_z, which is a third measure of surface roughness, is a ten-point parametric value that compare average high peaks and low troughs [14]. This method is more sensitive to occasional spread in surface defects, which is one of the values with the most impact to fatigue strength, described in equation 9.

$$R_z = \frac{1}{n}\left(\sum_{i=1}^{n} p_i + \sum_{i=1}^{n} v_i\right) \tag{9}$$

2.8 Etching

Etching is a method that enhances the microstructure by means of selective corrosion. The corrosion reveals the grain boundaries, or solidification structure, and facilitates measurement of the grain size, which is hard to see after only polishing [15]. Hardness testing and evaluation of the porosity, must be done before etching.

Chemical etching is done with a corrosive solution that corrodes regions of high susceptibility [16]. Electrolytic etching is a form of chemical etching, but with an electric current applied. For electrolytic etching to work the material of the specimen need to be electrically conductive, which stainless steel 316L is.

2.9 Hall-Petch strengthening

The complex microstructure created in the DMLS process, generate small sub-grains and larger grains. The size of the grains affects the mechanical properties. A phenomenon called Hall-Petch strengthening, or grain-boundary strengthening, means in short that changing the average grain size affect the materials strength. There are two reasons to why a change in grain size affects the yield strength and influence the dislocation movement.

Dislocation travel through the lattice with the help of a relatively small stress applied. An obstacle that halts this movement and requires a great amount of force to overcome is called a pinning point. Grain boundaries act as such obstacles. Grains have different orientation and for a dislocation to travel through the boundary between grains, it needs to change direction, which requires more energy. Furthermore, boundaries are less ordered then inside grains, which prevent dislocations moving in a continuous slip plane.

3. METHOD

The methods used in this study are accounted for in this chapter and will act as a guide for further investigation and support for replication of this study.

3.1 Basic structure and samples

To better understand what planes, designations- and axis used in the study, see *Figure 3.1*.

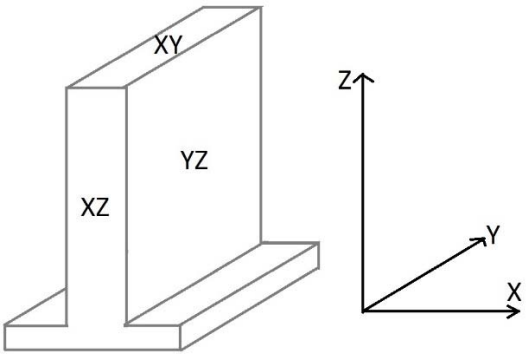

Figure 3.1: A sample with indicated planes and axis.

A test matrix was created to differentiate the different samples and the positions on those specific samples, see *Table 3.1.*

Table 3.1: Test matrix of nine individual samples and their position.

Material	Powder	Parameters	Wall thickness	Position (Z)	Plane	Spacing	ID
316L	EOS	EOS Standard	0,2 mm	Top (T)	XZ	5 mm	316L_EOS_Z02_T
316L	EOS	EOS Standard	0,2 mm	Middle (M)	XZ	5 mm	316L_EOS_Z02_M
316L	EOS	EOS Standard	0,2 mm	Bottom (B)	XZ	5 mm	316L_EOS_Z02_B
316L	EOS	EOS Standard	0,4 mm	Top (T)	XZ	5 mm	316L_EOS_Z04_T
316L	EOS	EOS Standard	0,4 mm	Middle (M)	XZ	5 mm	316L_EOS_Z04_M
316L	EOS	EOS Standard	0,4 mm	Bottom (B)	XZ	5 mm	316L_EOS_Z04_B
316L	EOS	EOS Standard	0,6 mm	Top (T)	XZ	5 mm	316L_EOS_Z06_T
316L	EOS	EOS Standard	0,6 mm	Middle (M)	XZ	5 mm	316L_EOS_Z06_M
316L	EOS	EOS Standard	0,6 mm	Bottom (B)	XZ	5 mm	316L_EOS_Z06_B
316L	EOS	EOS Standard	0,8 mm	Top (T)	XZ	5 mm	316L_EOS_Z08_T
316L	EOS	EOS Standard	0,8 mm	Middle (M)	XZ	5 mm	316L_EOS_Z08_M
316L	EOS	EOS Standard	0,8 mm	Bottom (B)	XZ	5 mm	316L_EOS_Z08_B
316L	EOS	EOS Standard	1,0 mm	Top (T)	XZ	5 mm	316L_EOS_Z10_T
316L	EOS	EOS Standard	1,0 mm	Middle (M)	XZ	5 mm	316L_EOS_Z10_M
316L	EOS	EOS Standard	1,0 mm	Bottom (B)	XZ	5 mm	316L_EOS_Z10_B
316L	EOS	EOS Standard	1,5 mm	Top (T)	XZ	5 mm	316L_EOS_Z15_T
316L	EOS	EOS Standard	1,5 mm	Middle (M)	XZ	5 mm	316L_EOS_Z15_M
316L	EOS	EOS Standard	1,5 mm	Bottom (B)	XZ	5 mm	316L_EOS_Z15_B
316L	EOS	EOS Standard	2,0 mm	Top (T)	XZ	5 mm	316L_EOS_Z20_T
316L	EOS	EOS Standard	2,0 mm	Middle (M)	XZ	5 mm	316L_EOS_Z20_M
316L	EOS	EOS Standard	2,0 mm	Bottom (B)	XZ	5 mm	316L_EOS_Z20_B
316L	EOS	EOS Standard	2,5 mm	Top (T)	XZ	5 mm	316L_EOS_Z25_T
316L	EOS	EOS Standard	2,5 mm	Middle (M)	XZ	5 mm	316L_EOS_Z25_M
316L	EOS	EOS Standard	2,5 mm	Bottom (B)	XZ	5 mm	316L_EOS_Z25_B
316L	EOS	EOS Standard	3,0 mm	Top (T)	XZ	5 mm	316L_EOS_Z30_T
316L	EOS	EOS Standard	3,0 mm	Middle (M)	XZ	5 mm	316L_EOS_Z30_M
316L	EOS	EOS Standard	3,0 mm	Bottom (B)	XZ	5 mm	316L_EOS_Z30_B
* Extra ID-endings can occur due to position of the sample (L, M, R) meaning Left, Middle, Right as sample is seen in pict							

A basic structure, consisting of nine different walls with varying wall thicknesses, between 0,2 mm to 3 mm, were created to analyze the porosity, evaluate the hardness and observe the behavior of the microstructure, see *Figure 3.2.* The parts were built with EOS-316L powder utilizing standard EOS-process parameters.

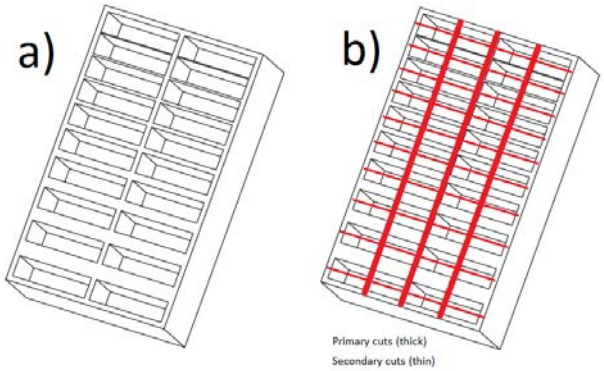

Figure 3.2: a) Basic structure. b) Three thicker primary cutting lines and ten thinner secondary cuts.

To make sure the ribs were not deformed, a precision cutting machine, ATM Brillant 220, was used together with a 0.6 mm thick cut of wheel used for softer ferrous materials. The precision cutting machine, together with a thin cutting wheel and proper parameters, can cool the cut to maintain the true structure of the material. A cutting speed of 10 mm/min was used to minimize embedded plastic deformation.

The basic structure was first sectioned with three primary cuts, ending with four base sections, consisting of nine possible samples (*Figure 3.3*), which gave a total of 36 possible samples. As a first attempt, one base section was cut into three separate sample sections, A (0.2 mm, 0.4 mm and 0.6 mm), B (0.8 mm, 1.0 mm and 1.5 mm) and C (2.0 mm, 2.5 mm and 3.0 mm). As seen in *Figure 3.4*, the sectioning led to a deformation of the thinner walls due to the high temperature and the high hydrostatic pressure during the hot mounting process. By cutting the samples individually, this effect could be minimized or counteracted (*Figure 3.5*). The plane that is later observed is the xz-plane, which also is the building direction. To reduce thermal impact, the observation plane is in the middle of the wall.

Figure 3.3: Basic structure after two primary cuts.

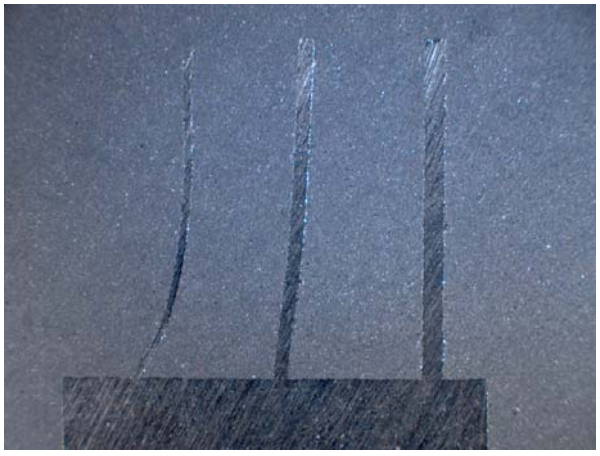

Figure 3.4: Mounted and deformed section sample showing Z02 (left) Z04 (middle) Z06 (right).

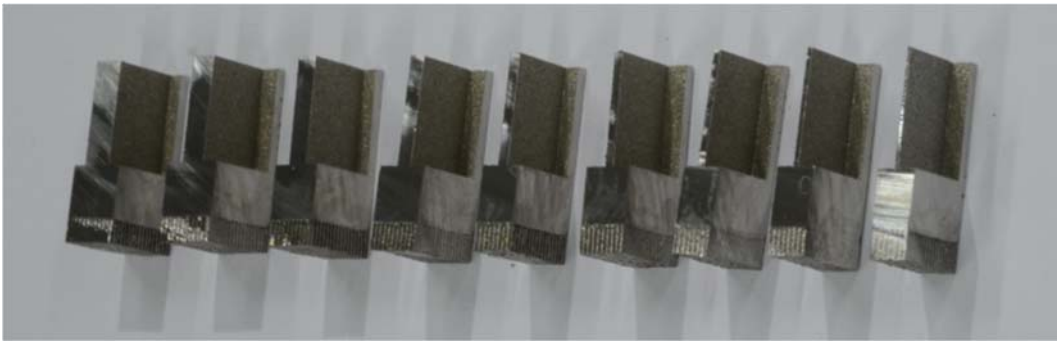

Figure 3.5: Samples after both primary and secondary cut.

3.2 Sample preparation

Sample preparation is needed for easier observation of both the macrostructure and the microstructure of the material, the samples were therefore first mounted. A hot mounting process is quick and secure for materials that can handle the temperature and pressure. After mounting, the samples are placed in a holder and grinded and followed by polishing.

A recipe for the whole sample preparation can be read in *Appendix 1*. All grinding and polishing is done in AbraPlan-20 (first rough grinding step) and AbraPol-20 (second rough grinding step to the finished polished sample). The holder is rotating with a speed of 150 rpm counter clockwise while the stone/disc is moving at 500/300/150 rpm counter clockwise depending of process.

3.2.1 Hot mounting

The samples were mounted in an epoxy based resin, ending up with a Ø 40 mm mounted sample. The epoxy based resin from Struers, called DuroFast, is a hard resin, used to retain edge definition of the sample. It is also preferable as a resin when hardness testing with higher loads is performed. One disadvantage of the resin is the fact that it is not conducting, which is not preferable for an analysis done in SEM. One row of samples where therefore mounted into a bakelite resin which is conductive, called PolyFast, with (Ø 30 mm). The PolyFast resin was also showing better polishing results.

3.2.2 Rough grinding

To secure a flat surface, the samples were rough grinded, with a #150 (FEPA) water cooled stone and a sample force of 30-40 N, depending of sample diameter. Due to a controlled and light handling of the material during the cutting process, the disforestation could be limited to 200 µm. Result can be seen in *Figure 3.6*.

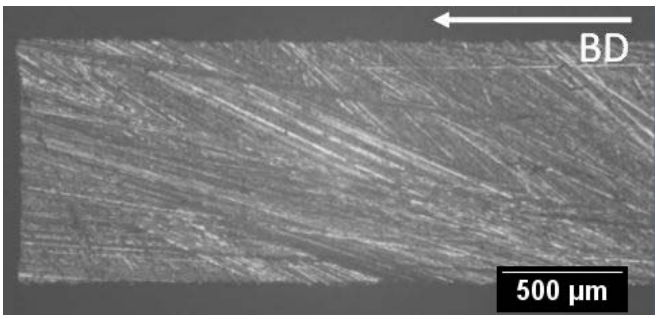

Figure 3.6: Rough grinded (#150) sample with 25x magnification.

For a firm process, a second rough grinding step was completed. The disk used was a water cooled Piano #220 (FEPA) which is a resin bonded diamond disc. Instead of removal, this program is bound by time of 1 minute. A sample force of 30-40 N (depending of sample diameter) is used during this process. The result after a second rough grinding step is seen in *Figure 3.7*.

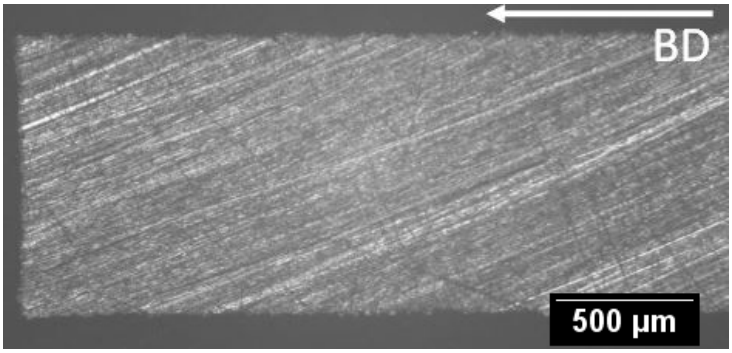

Figure 3.7: Rough grinded (#220) sample with 25x magnification.

3.2.3 Fine grinding

The fine grinding step is done with a MD-Largo disc, which is a full composite disk. Automatic adding of a coolant and suspension during the process ensures the right conditions. The lubricant (Struers DP-lubricant blue) is alcohol based to ensure the right cooling and reduce smudging during the process. The abrasive (Struers DP-Suspension 9 µm) is a diamond suspension containing polycrystalline diamonds with a maximum size of 9 µm. The process is going on for 4 minutes with a sample force of 30-40 N. Result after fine grinding is seen in *Figure 3.8.*

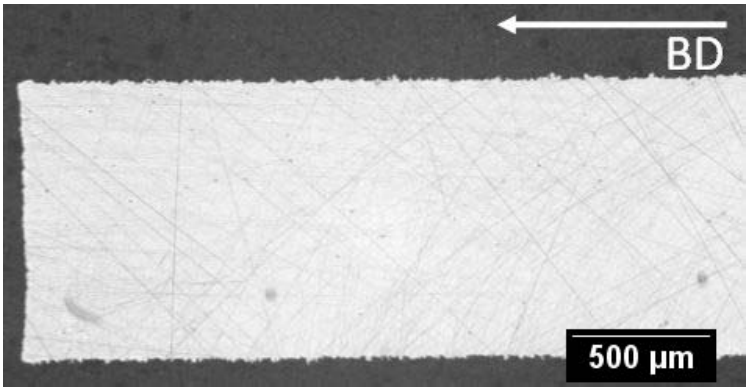

Figure 3.8: Fine grinded (9 µm) sample with 25x magnification.

3.2.4 Polishing

The first of two polishing steps are done using a Struers MD-Dac, a woven acetate surface which is considered as a hard disc to retain edge definition on the sample. The lubricant and abrasive are automatically added as before, an alcohol based Struers DP-lubricant blue, together with a finer abrasive, Stuers DP-suspension P 3 µm. The process is 5 minutes long and the force on each sample is 20-25 N. As seen in *Figure 3.9*, even if the surface looks scratch free after this step, a dark field filter reveals a lot of small scratches on the surface.

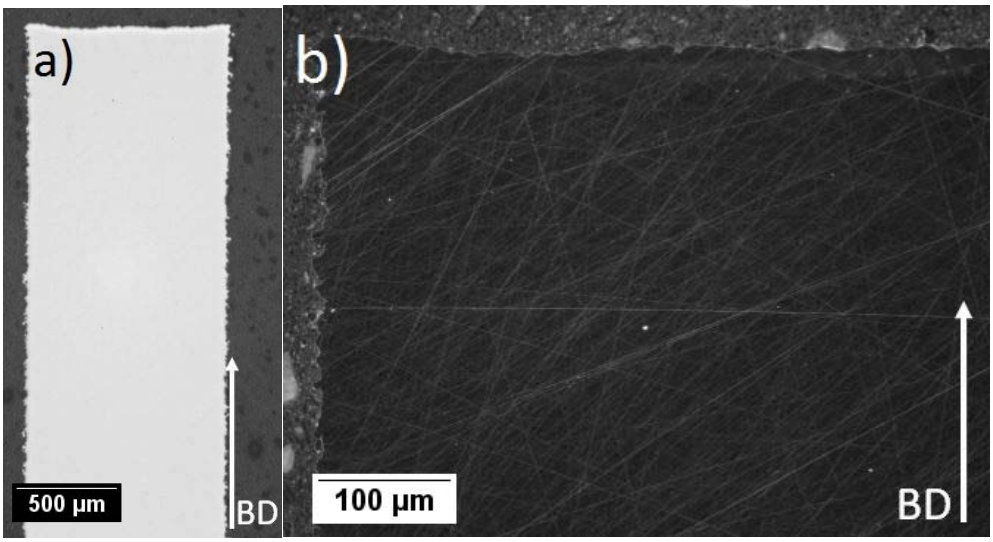

Figure 3.9: Polished (3 µm) sample. a) 25x magnification BF. b) 100x magnification DF.

This is a second optional final polishing step. The disc is now switched to a Struers MD-Nap which is used together with the same lubricant as before. The disc is now considered to be a very soft disc, which is used to create a scratch free surface. The abrasive is a Struers DP-suspension P 1 µm and is used for 2 minutes with 20-25 N sample force. After the automatic cleaning process, the sample is cleaned in alcohol to reduce drying stains. The result is a scratch free surface, a result that in a light microscope is similar to the one seen in *Figure 3.10*.

3.2.5 Oxide polishing

The final step of the sample preparation process is oxide polishing, which can be used in several different ways. The oxide comes in two different variants and can be performed after the 3 µm polishing step, meaning that the 1 µm-polishing step is not needed. The oxide polishing suspension is adulterated with water and works both as abrasive and lubricant and is used together with Struers MD-Chem disc, which is a porous neoprene disc. The disc is very soft, which create risks of both edge rounding and relief. The later can be useful, which can be seen later.

OP-U is one of two oxide-polishing suspensions and contains 0.04 µm silica oxide particles. The use of this suspension is mainly for samples that are going through a SEM analysis. To reduce the risks of edge rounding and relief, this polishing step is done for a minute with a sample force of 15-20 N. The result is a scratch free surface (*Figure 3.10*) up to very high magnification without relief. This process was used before porosity analysis to ensure a good polished result.

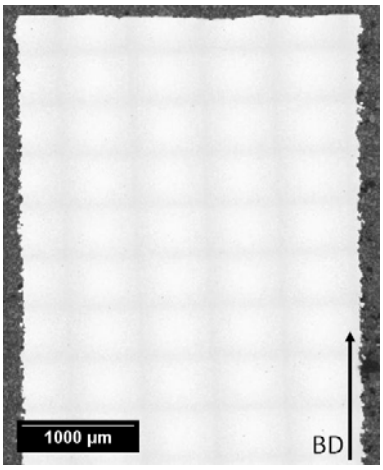

Figure 3.10: Polished (0,04 µm OP-U) sample with 25x magnification.

OP-S is another silica oxide based suspension containing particles with a size of 0.04 µm. The main purpose of this oxide polishing step is to get a relief due to longer polishing time and that the process is both abrasive and oxidative. The suspension is a light etchant and is therefore a way of etching the sample right from polishing. This process was used to see if the result might discover some of the questions asked. The relief makes it hard to look at the structure at high magnification due to low depth of field, but is a good way to evaluate the structure on macro-level. The polishing time for this kind of samples was around 3 minutes with a sample force of 15-20 N. The relief is easy to spot, as seen in (*Figure 3.11*), if it is compared with the one from the OP-U polishing result.

Figure 3.11: Polished (0.04 µm OP-S) sample with 25x magnification.

3.3 Porosity

The porosity of the samples was investigated at Volvo Materials Technology with Leica DMi8. Each sample pictures were taken and stitched together into a full image. This was performed at a magnification of 200 times. An additional image with a higher magnification was conducted for some areas.

3.4 Hardness testing

The hardness testing is performed in a Struers DuroScan with a Vickers indenter. Depending on wall thickness, load of 0,1 kgf (HV 0,1), 0,2 kgf (HV 0,2) and 0,3 kgf (HV 0,3) were used for measurement of Vickers. Five to ten indentations were made at three different positions of the sample to be able to do a statistic research of the result (*Figure 3.12* and *Figure 3.13*). An edge measurement was done where a matrix of indentations was placed on the edges of the material.

Figure 3.12: Positioning of indentations for sample hardness testing.

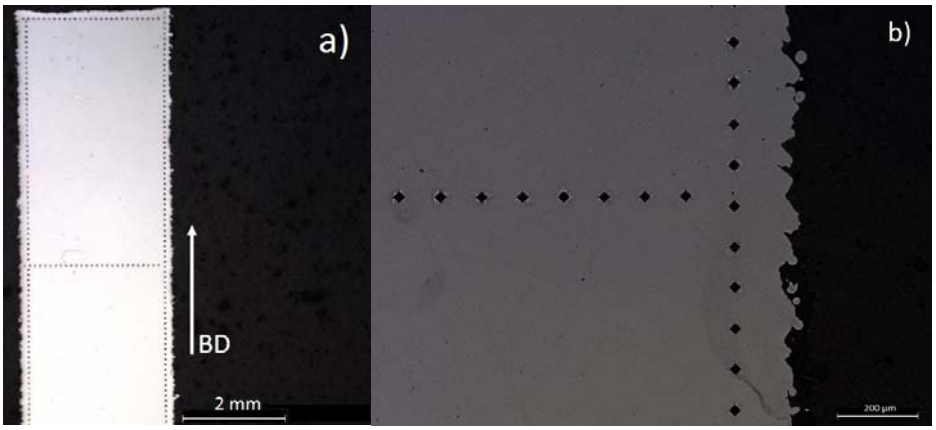

Figure 3.13: Positioning of indentations for edge hardness testing. a) Low magnification. b) High magnification.

3.5 Etching

The samples electrochemically etched, in newly polished condition to minimize the risk of oxidation on the surface. A piece of platinum was used for the cathode of the current instead of tweezers. This accelerated the process speed and made the grain boundaries visible. Some samples were repolished and etched this way again, due to them being over etched the first time. For studying the microstructure after etching Leica DMi8 were used. All samples were magnified 200 times.

4. RESULTS AND DISCUSSION

All results obtained from the methods applied will be described and presented in this chapter. The results are also discussed to raise the relevance and creditability of the results presented.

4.1 Porosity

4.1.1 Spherical pores

Spherical pores are by far the most common in all samples, regardless of wall thickness. A large spherical pore; with a diameter of approximately 12 µm, can be seen in *Figure 4.1*. Pores of this size are a minority, but exist through all the samples. It is reasonable to assume that the spherical pores are created by entrapped gas inside the powder based on the size and their spherical shape.

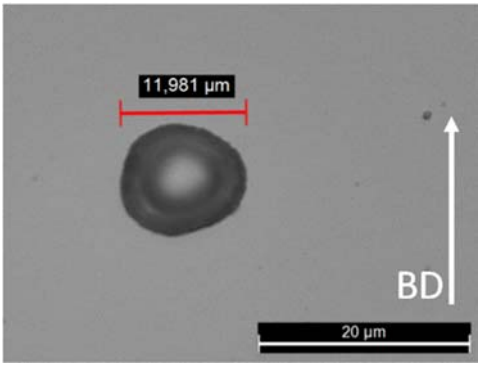

Figure 4.1: Spherical pore from sample Z25.

4.1.2 Non-spherical pores

In *Figure 4.2*, a non-spherical pore is shown, which has a length of 133 µm and width of 67 µm. This size of porosity could have large impact on the mechanical properties if a large amount is found. Since only a small number of large pores was found it is rational to assume that this will not have any large effect on the mechanical properties. Furthermore, due to its shape it can be assumed that this type of defect most probably was created due to lack of fusion or lack of packing of powder during the processing.

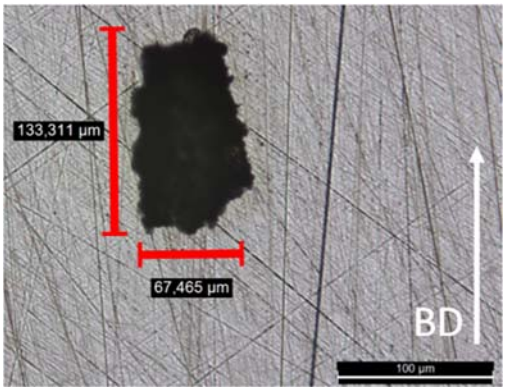

Figure 4.2: Non-spherical pore from sample Z15.

4.1.3 Wall thickness and porosity

In the study, samples range from 0.2 mm to 3 mm in thickness. Seeing as the samples are thinner there could be some differences in porosity compared to the study done by Yusuf et al. [12]. However, investigation of the porosity of each wall thickness makes it clear that the porosity is

evenly distributed through the entire length. It appears that the wall thickness does not have any effect of what type of pores created in the component, both spherical and low amount of non-spherical pores are found for all thicknesses. Since overall porosity is very low this indicates good part quality. *Figure 4.3* shows three different wall thicknesses for which no trends can be observed regarding the porosity. For a complete view over the porosity in all the samples, in their full length, see Appendix 2.

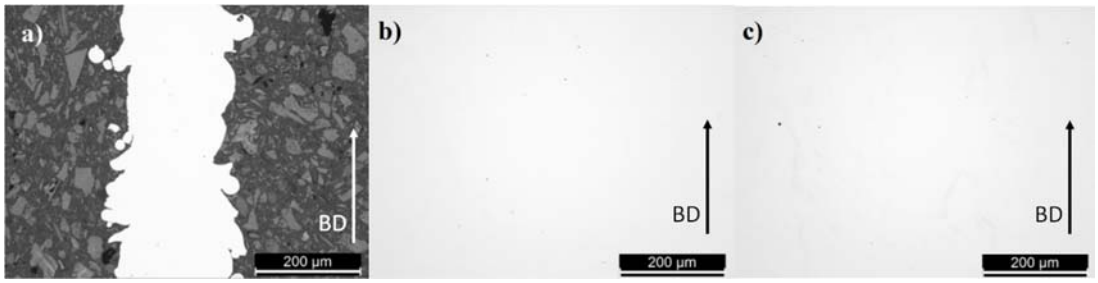

Figure 4.3: Porosity in three different wall thicknesses. a) Sample Z02 b) Sample Z15 c) Sample Z30.

The overall assumption is that the porosity distribution appears the same regardless of the wall thickness. However, a more valid study and precise method need to be used, to fully clarify this. There is no study found, regarding the wall thickness and it is therefore hard to compare these results with other studies. Pores will appear in this material but if they are small with an independent spread, the effects will not be enlarged.

4.2 Hardness testing

The hardness testing was performed to find out if the wall thickness and build height affected the hardness of the material. The indentation series was made at the top, middle and bottom on every sample, to ensure a statistic value for the position hardness, see *Figure 4.4.* The full data sheet for all the measurements can be found in *Appendix 3*.

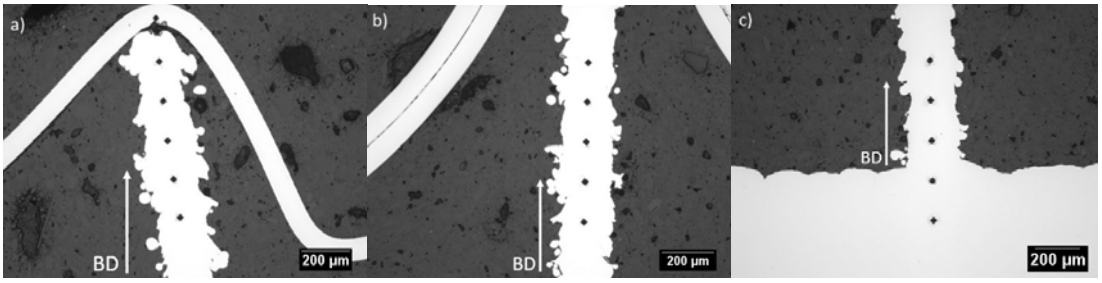

Figure 4.4: Indentation on a) Top. b) Middle and c) Bottom of the Z02 sample.

4.2.1 Sample average

The sample average is the mean hardness value for a specific sample together with the standard deviation for that specific sample and measurement. As seen in *Figure 4.5*, the average sample value for the whole sample structure spreads from 227.1 (Z04) to 247.6 HV (Z20) with standard deviations of 11.2 HV (Z04) and 12.3 HV (Z20), respectively, resulting in an overlapping range of measurement. The result shown in *Figure 4.5* indicates that there is no statistically significant difference in hardness depending on the wall thickness.

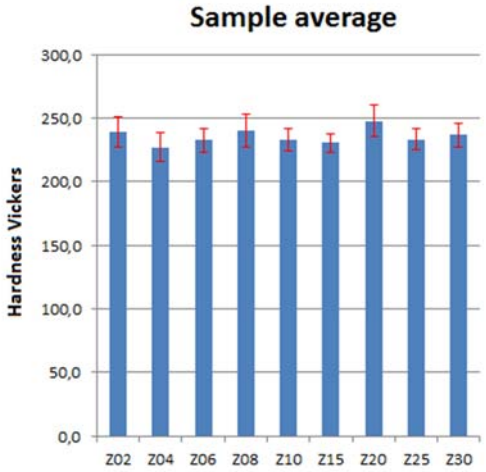

Figure 4.5: Chart of the sample's average hardness.

If the wall thickness would affect the hardness, there would be more visible trends. Due to the nature of the samples, and the rules of Vickers indentations, the method did vary, which may affect the result of the measurements owing to micro/macro characteristics.

As seen in *Appendix 3* (full data sheet of measurement) under Z10, a lot of the measurements were unapproved by the cause of differentiation of the indentation diagonal, see *Figure 4.6*. To solve this problem, a higher load was used, resulting in fewer unapproved indentions. The light load was used for edge hardness measurements, where there were no tendencies for many unapproved indentations.

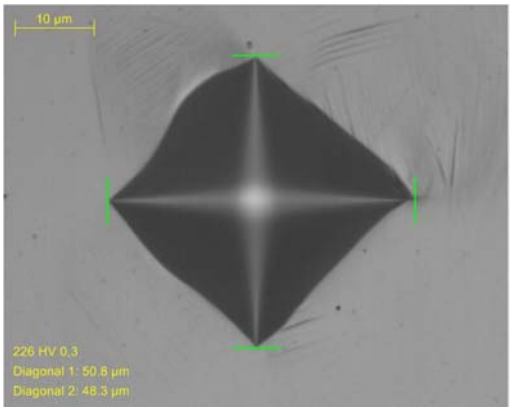

Figure 4.6: Diagonal problem during hardness testing. As seen, diagonal 1 is longer than diagonal 2.

As seen in *Appendix 3* most of the unapproved indentions (16 of 18) were unapproved because of that diagonal 1 was longer than diagonal 2. This might indicate that there are differences in the micromechanical properties of the material, which can be something to investigate further.

To adjust and improve the method of measurement, it would be preferable to measure on another plane that gives a larger surface of measurement to use a higher force. This would make it possible to measure the macrohardness over a full range of samples. It may also enhance the consistency of the measurement and therefore also reduce the impact of suspected mechanical properties in different directions, leaving a result that shows if the material tends to be

homogenous or not. To preclude edge effects, the measurement should be done in the middle of the evaluated wall thickness.

4.2.2 Position average

As seen in *Figure 4.7*, an average value of the hardness of a specific position on the different samples and the standard deviation of those samples is presented. As in the case of wall thickness, there are no clear results that indicate that wall thickness would contribute to differences in hardness, due to building height.

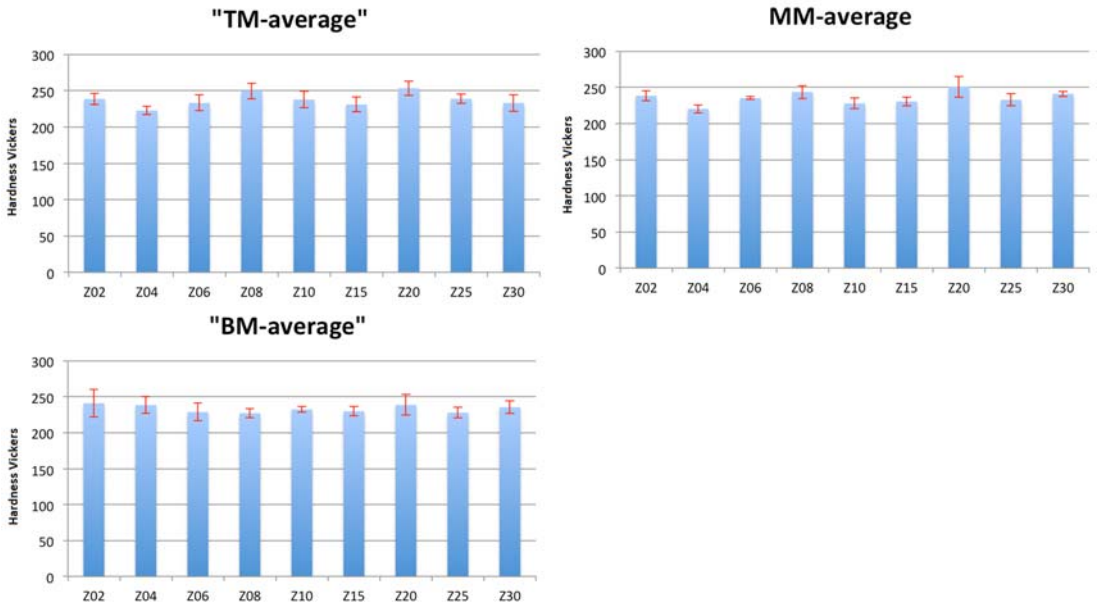

Figure 4.7: Charts of average sample hardness. a) Top average. b) Middle average. c) Bottom average.

4.2.3 Total average

When combining all the statistical data into a total average, *Figure 4.8*, the results indicate that there is no clear correlation between hardness and either wall thickness or build height. A total sample average of 235.9±11.4 HV gives a range between 224.5 to 247.3 HV, which covers most of the sample average hardness. This points out that no individual sample is divergent.

The same result is found when comparing the total average position hardness with average sample position hardness. The TM-position (top-middle) has a hardness of 238±12.17 HV, which results in a rage of 225.3 HV to 250.7 HV. This range covers most of the average sample positions hardness without involving the standard deviation of those specific positions.

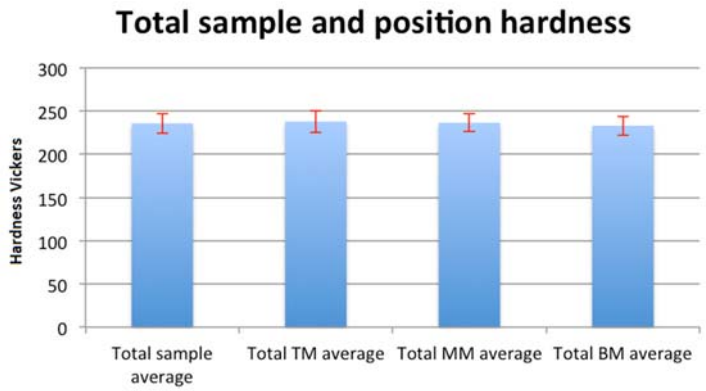

Figure 4.8: Chart of total average hardness for all samples.

4.2.4 Edge hardness

To see if there were any surface effects linked to hardness, a few indentations were taken both along the edge (building direction) and across the building direction (through the structure) on the Z30 sample, see *Figure 4.9*. There were no obvious differences between the hardness that was measured and the statistical data above. The measurements were therefore not worked with and continued throughout all the samples.

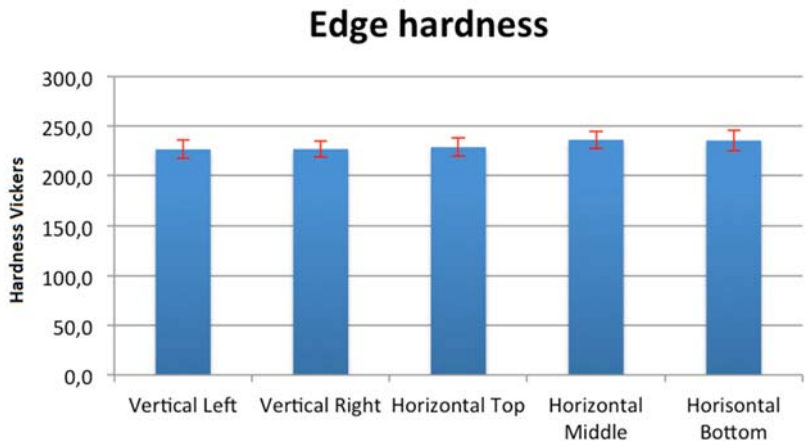

Figure 4.9: Chart of edge hardness.

The results presented are in fact expected and ensures that there are no effects which affect the micro hardness of the material. It does answer the research question if specified to micro hardness. Because of the process and material itself, the hardness should not differ too much when it comes to wall thickness, position and surface measurements. No research which is specified in this way is found. Other hardness measurements by Wang et al. [9] have been done and show slightly higher microhardness, probably depending on process parameters and machine. The results here suggest a quite homogenous structure, which indicates that the hardness properties of the material will not be affected by the component itself.

4.3 Microstructure

4.3.1 Various microstructures across the surface

Along the surface of the xz-plane of all the samples, columnar sub-grains have grown in different directions, making the sub-grains appear as round, fibers or something in between.

The cellular structure can be seen as tubes, cut in different positions and angles. It appears that these sub-grains are either of a cellular structure or a cellular-dendritic structure with an absence of secondary dendritic arms [6].

In area B in *Figure 4.10 a)* the sub-grains appear as small and round, the red line in *Figure 4.10 b)* show schematically how the sub-grains are cut perpendicular to the growth direction, which makes appearance of the sub-grains seen in *Figure 4.10 a)*. However, some of these round structures appear larger, which can be seen by comparing area "B" and "C" in *Figure 4.10 a)*. The cellular microstructure look like needles, for AM manufactured 316L that are thicker towards their bottom and thinner at their top [15]. Depending on where the cells are cut, they are going to appear smaller or bigger in diameter, which can be seen by comparing there the line cuts in *Figure 4.10 b)* and *Figure 4.10 c)*, respectively, which divide the cells on different levels.

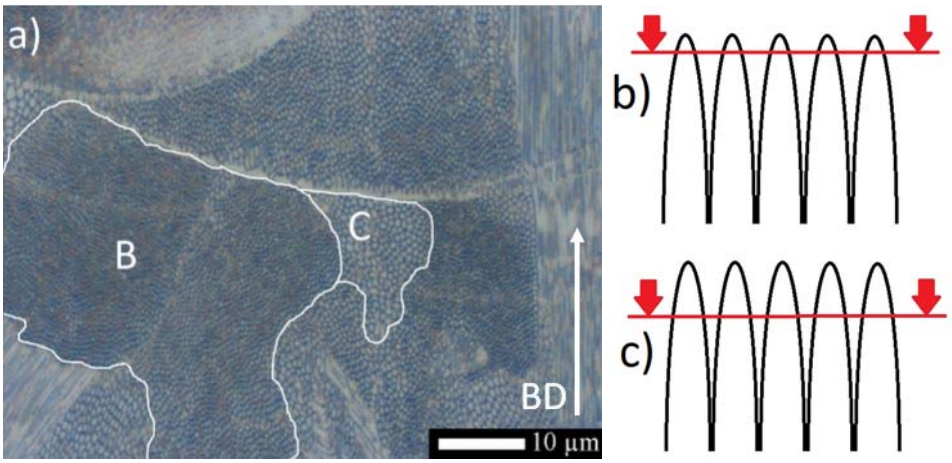

Figure 4.10: Microstructure cut perpendicular to growth direction. a) Shows the structure of the Z20 sample. b) Cutting line of structure in area B. c) Cutting line of structure in area C.

Area “B” in *Figure 4.11 a)* on the other hand shows the sub-grains looking long and pointed. This is the sides of the "needles" and is shown schematically by the line in *Figure 4.11 b)* which shows how the sub-grains are cut parallel to the sub-grains growth direction.

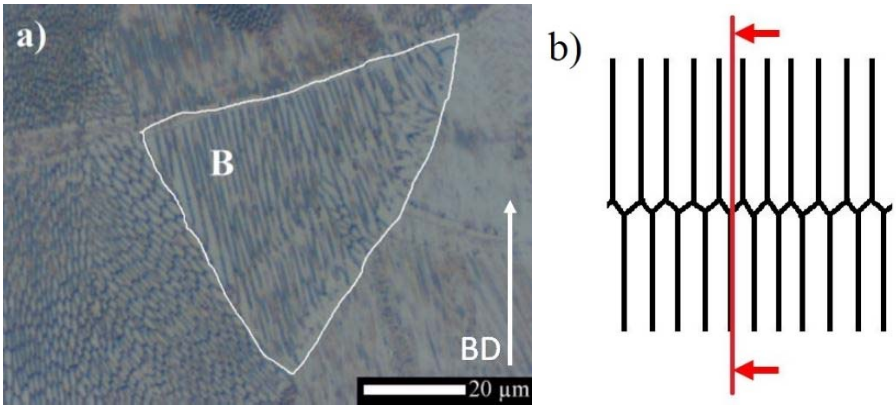

Figure 4.11: Microstructure cut parallel to growth direction. a) Shows the structure of the Z20 sample. b) Cutting line of structure in area B.

In *Figure 4.12 a)* the sub-grains have a nonspecific oblong shape that varies slightly in size. As evidenced by the line in *Figure 4.12 b)*, the sub-grains are cut diagonal to the grain direction.

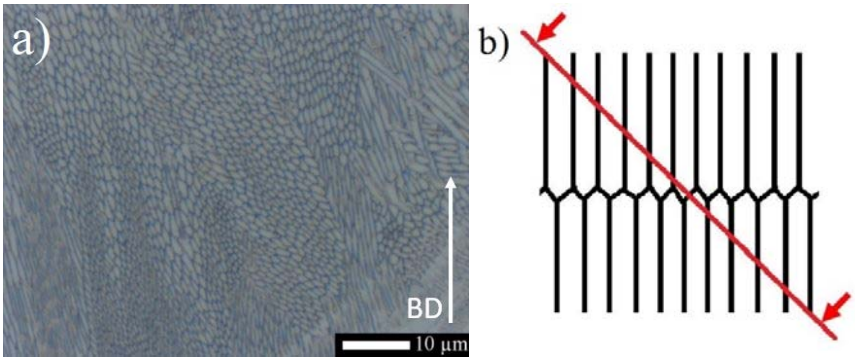

Figure 4.12: Microstructure cut diagonal to growth direction. A) Shows the structure of the Z20 sample. B) Cutting line of structure of structure.

Since the sub-grains themselves appear lighter in the optical microscope than the boundaries and as a diagonal cut maximize the area of the cut, the overall impression of the type of structure seen in *Figure 4.12 a)* is that it is lighter than the one seen in *Figure 4.10 a)* and *Figure 4.11 a)*. The reason the parallel cut is not the lightest depends on that fact that the cut does not always cut right through the sub-grain. It might as well cut just the surface of the sub-grain, giving an impression of slim sub-grains and thicker boundaries.

4.3.2 Solidification structure

The following section shows an out-take of the etched samples and their microstructure, for a full view of all samples see *Appendix 4*. As seen in *Figure 4.13 a)* there are parts of the structure that is perceived as lighter (*Figure 4.11* and *Figure 4.12)* and darker (*Figure 4.10*) areas. *Figure 4.13 b)* exaggerates this even more due to contrast manipulation of these areas. As can be seen, the darker areas tend to be found in the center of the section while the lighter areas are found close to the surface. It is also notable that the lighter areas are found between the darker areas, even in the middle of the section. It is also observed that the dark areas tend to be lightened when approaching the top surface of the sample. The darker and lighter areas are in fact a result of optical effects and appear in this way due to the orientation of the sub-grains.

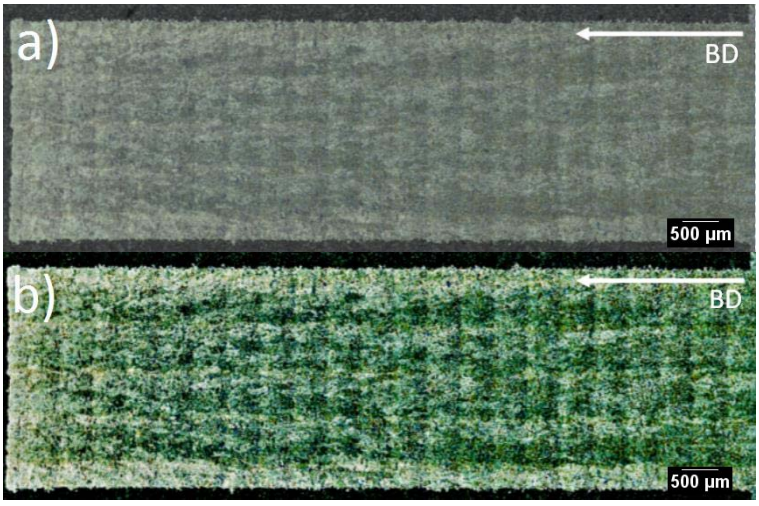

Figure 4.13: Section of sample Z30 showing the lighter and darker solidification structure. a) Original. b) Manipulated picture.

The variety of darker and lighter areas are found throughout the samples, and the effects can be seen from Z30 down to Z15, with gathered chunks of dark areas which is limited by dappled lighter areas in between as shown in *Figure 4.14*. The effects of light-dark-light phenomena clearly disappear when comparing the thicker samples (Z30 to Z15) with the medium thick samples (Z10 and Z08), which can be seen in *Figure 4.15*. The light areas are showing up more distinct and the darker chunks are not as continuous in the building direction as in the wider samples. When looking at the thinner rib sections, below 0.6 mm, the effects of darker areas are almost gone. There are a few smaller areas that appear dark but the effects seen in the widest samples are gone. The lighter areas are dominating the structure of these samples, as can be seen in *Figure 4.16*.

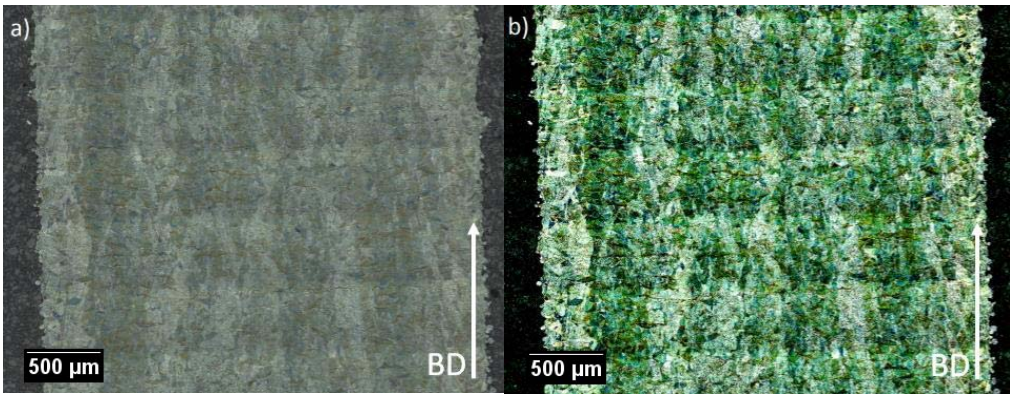

Figure 4.14: A magnified picture of the Z30 structure with light-dark-light phenomenon a) Original. b) Manipulated picture.

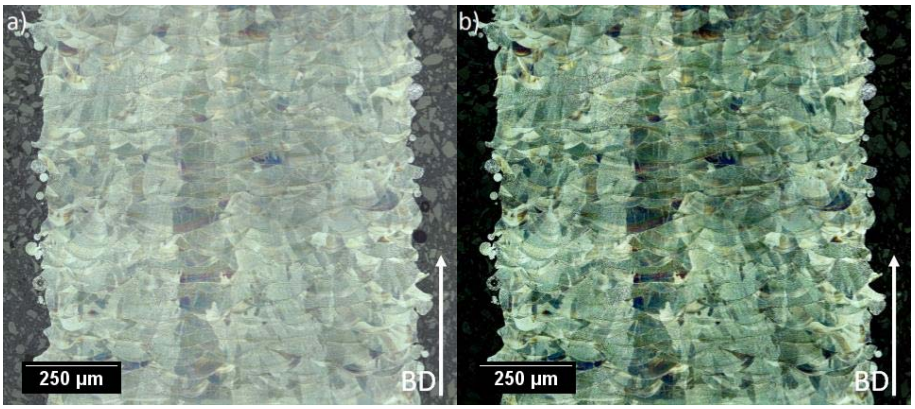

Figure 4.15: A magnified picture of the Z10 structure. a) Original. b) Manipulated picture.

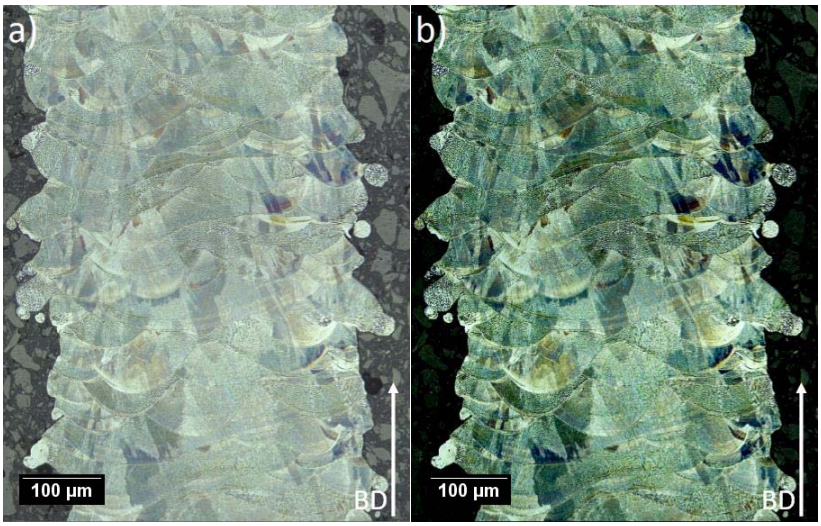

Figure 4.16: A magnified picture of the Z04 structure. a) Original. b) Manipulated picture.

The results hence indicate that the wall thickness does affect the microstructure of the material. Clear tendencies through the structure have though been observed. The darker and lighter areas are always stretched in the building direction in the same way as seen in the OP-S polished samples, see *Figure 3.11*. These findings indicate that the wall thickness might affect the heat flow and by that altering the solidification structure. Wang et al. [9] has illustrated with a heat flow plot of the melt pool. They also mentioned that former growth patterns are influencing the later structure built. To fully understand this phenomenon further investigation is needed, to confirm the root cause of the directional changes in the structure.

4.3.3 Edge defects

As can be seen in *Figure 4.17 a)* the sample has poor surface roughness in the vertical direction (building direction) compared to *Figure 4.17 b),* where the horizontal direction is perpendicular to the building direction. The surface roughness of the samples is not measured, but the differences are large. The surface finish plays as a key role when it comes to fatigue strength, were small differences can result in large impact. For instance, a tensile strength of 500 MPa [17] and a surface roughness of Ra 25.6 µm can result in a reduction factor of fatigue strength up to ~0.8 [14].

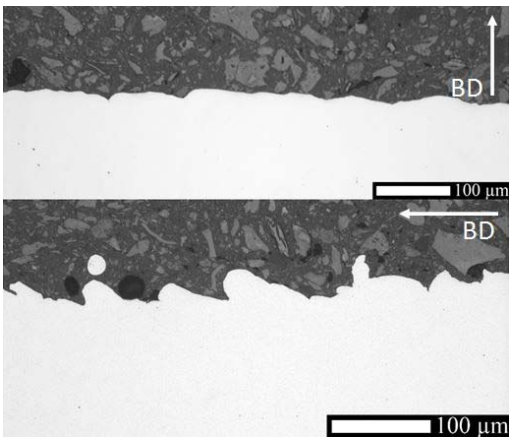

Figure 4.17: Differences in surface roughness at 200x magnification a) Rough surface parallel to BD. b) Finer surface perpendicular to BD.

All samples have evenly distributed roughness along the edge. These roughness characteristics seem to be created by mainly two types of mechanisms, un-molten grains and heat affected grains. In *Figure 4.20* an un-melted grain is shown. Within the grain a distinct dendritic structure with secondary dendritic arms has remain untouched by the DMLS process. In *Figure 4.19* a heat affected grain is shown. Compared to the un-molten grain, this grain has a smoother surface and is attached more firmly upon the sample wall. It has also lost the gas-atomized grains' dendritic structure and appears to have either a cellular structure or a cellular-dendritic structure without secondary dendritic arms. The solidification structures that can be seen in the un-molted grain come from the solidification structure from the gas atomization. The difference to the heat affected grain in turn come from an elimination of this solidification structure, resulting in the homogenizing in the heataffected grain.

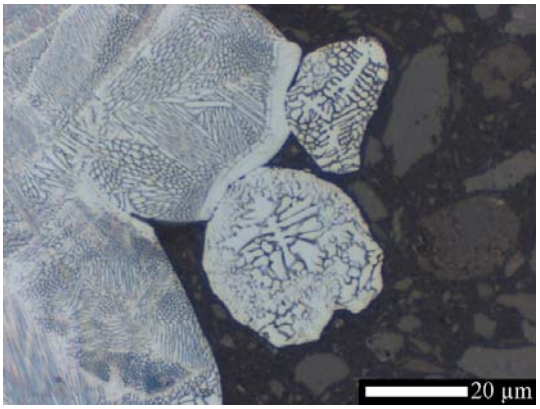

Figure 4.18: Unmolten metal power at the surface of the structure.

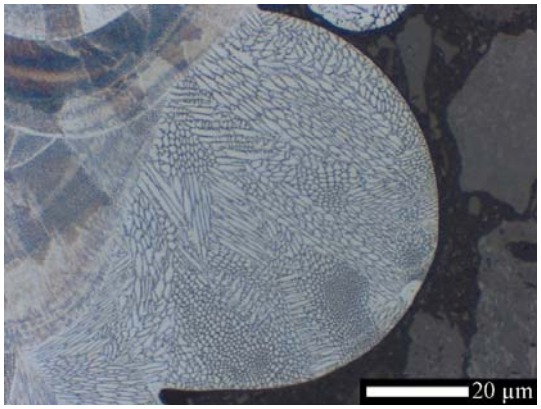

Figure 4.19: Partially melted powder at the surface of the structure.

In comparison between the microstructure shown in *Figure 4.19* and the microstructure of *Figure 4.10 a), Figure 4.11 a)* and *Figure 4.12 a)*, the structure in *Figure 4.19* is significantly lighter and less orderly.

Surface roughness is an important problem in many processes. Even here, the fact that the thinnest wall thickness is 0.2 mm indicates that the surface roughness plays a key role in the mechanical properties of this structure. This is due to the "amount" of surface area in relation to the other structural area. The total section area of the Z02 sample is 2 mm^2 with a surface length of 20.2 mm (10,1 mm per mm^2), while our largest sample, Z30, has a section area of 30 mm^2 together with a 23 mm surface length (0,77 mm per mm^2). These comparisons are important to have in mind when calculating fatigue problems and therefore not favorable when manufacturing a component intended for fatigue loading.

4.3.4 Melt pools

The profile of the melt pools, as can be seen in *Figure 4.20 a),* is a result of the laser going along the y-axis. The melt pool profile of the xy- and yz-planes will have a completely different appearance, as illustrated by Yusuf et al. [12].

The laser beam does not only heat the top layer of powder, but also reach layers further down that have been molten earlier. The melt pool that is observed is therefore a result of this re-melting of material a few layers beneath the new powder bed. This will be processed for each layer and will eventually create the white arcs in a distinctive fish-scale pattern. This can be seen in *Figure 4.20 b),* as clear cuts through the rest of microstructure.

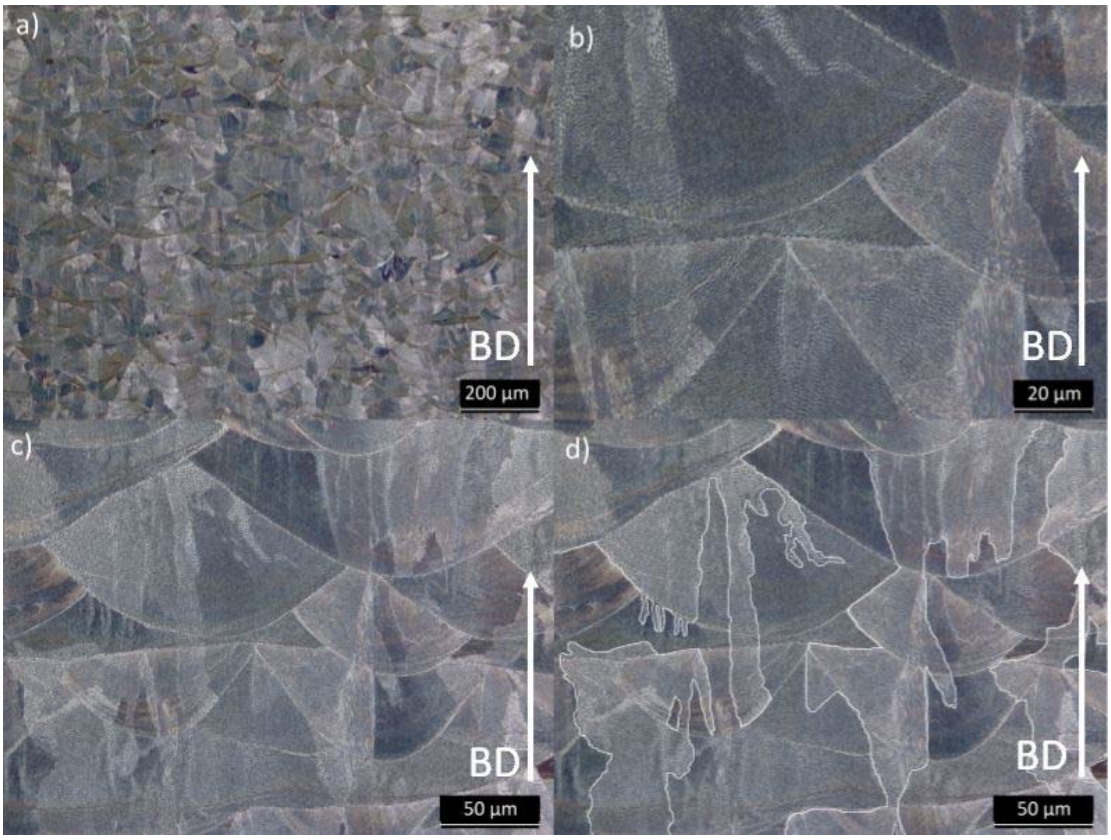

Figure 4.20: Melting pools shown in a) 100x magnification. b) 1000x magnification. c) 500x magnification. d) 500x magnification with circled solidification structures.

The arcs can be seen even clearer in higher magnification in *Figure 4.20 c)*, were the cellular-dendritic structure is not interrupted by the boundaries. The melt pool boundaries might act as pinning points and obstruct dislocations, and therefore strengthen the material. This is the same as the idea behind Hall-Petch strengthening. However, since a tensile test has not been done in this study, this cannot be confirmed.

In *Figure 4.20 d)* the solidification structure has been made clearer compared to *Figure 4.20 c),* which makes it more easily seen that the melt pool boundaries do not interfere with the solidification structure. In one single melt pool, dark and light areas can occur together. Since the lighter and darker areas depend on whatever direction the sub-grains grow into the xz-plane or across it, a conclusion could be that different directions exist in the same melt pool [18].

Since the laser beam re-melts several layers further down as it melts the powder layer at the top, it might explain why the solidification structure is not discontinued by the melt pool boundaries. As the laser beam does not reach further then the melt pool profile display in *Figure 4.20*, it will heat the surrounding areas, making the solidification structure follow the heat gradient.

5. CONCLUSIONS

This study shows that the fabricated components in 316L stainless steel, fabricated by means of powder-bed fusion with laser (DLMS) have high relative density, meaning low numbers of pores as well as small sized pores. The results indicate that there is no connection between wall thickness and porosity. This means that the wall thickness is not an issue regarding the porosity and therefore does not need to be included in any design limitations in this respect.

It can also be concluded that there is no correlation between wall thickness and hardness. Neither are there any correlation between build height and hardness. Furthermore, no edge effects were found, since the hardness close to the surface did not differ with the hardness of the samples in any significant way. The results were expected due to the unaltered manufacturing process. Cooling rates and solidification processes are similar for the whole structure and the material itself does undergo phase transformation upon solidification and cooling to full austenitic steel, which will have quite the same properties. The overall conclusion is that the measurements show homogenous micro-hardness results.

The study still reveals that there are differences in the microstructure when comparing different wall thicknesses. In samples of between 1.5-3 mm wall thicknesses there are a variety of darker and lighter areas found throughout. This phenomenon starts to disappear for smaller thicknesses at between 0.8-1 mm and is almost gone, with an exception of a few dark small areas, for thicknesses of between 0.2-0.6 mm. It can therefore be concluded that there is a clear difference in microstructure between wall thickness above 1 mm compared to walls thinner than 0.8 mm.

It is quite easy to spot the breaking point of structural orientation which can be useful together with further investigation of structural orientation and its correlation to mechanical properties. However, the effects of these differences and the importance of having specific orientation is still unclear. It can be concluded that design rules need to be taking to account the rib thicknesses due to the microstructure when the ribs are under 1 mm. Tough, it is still difficult to be more specific for design limitations based on these results.

In terms of edge defects the roughness is not affected by the wall thickness. However, for thinner walls there are more surface area compared the other structural area, which might be problematic in creating design rules. It is well known that the microstructure as well as surface roughness is factors for the mechanical properties. As the results point towards different directional tendencies, the mechanical properties as yield strength and tensile strength could be affected by these directional alterations. This could therefore be a factor when setting up design limitations.

5.1 Suggestions for further investigation

Owing to a small number of pores, a complete porosity study was not performed. If the study were to be taken further, a complete porosity investigation might be needed. The selected method for characterizing porosity only shows a small fraction of the total volume. Therefore, it should be noted that a more sophisticated method is needed to establish statistically approved results. There would also be preferable to use statistics in different sections of a full wall length to ensure the results of this study.

The method used for the microhardness measurements is certified and is done according to standard measurements and therefore the results should be sufficient. Nonetheless, further hardness measurement should be done to establish the macro hardness of the samples. Another

plane e.g. the yz-plane could be a useful complement for these measurements. There is also a possibility to use other methods of measurements, e.g. Knoop.

As have been concluded there is clear difference in microstructure for wall thicknesses about 1 mm compared to walls thinner than 0.8 mm. However, to pinpoint exactly were the microstructure start to change due to wall thickness, a more extensive study need to be done. A suggestion would be to evaluate walls between 0.2-1.5 mm more closely, with less spacing than in this study. The focus has been to evaluate the solidification structure together with sub-grains in this study. For a better comprehension of the microstructures behavior, an electron beam scattering diffraction (EBSD) analysis should be done to determine the crystallographic grains and their boundaries. This would give further understanding of the solidification and microstructure characteristics differences between light and dark appearing areas in optical microscopys.

References

[1] I. Gibson and D. Rosen, *Additive Manufacturing Technologies*, 2nd ed. Springer, 2015.

[2] K. Saeidi, *Kamran Saeidi Doctoral Thesis 2016*, Stockholm University, 2016.

[3] W. E. Frazier, "Metal Additive Manufacturing : A Review," vol. 23, no. June, pp. 1917–1928, Springer, 2014.

[4] C. Y. Yap, C. K. Chua, Z. L. Dong, Z. H. Liu, D. Q. Zhang, and L. E. Loh, "APPLIED PHYSICS REVIEWS — FOCUSED REVIEW Review of selective laser melting : Materials and applications," vol. 12004, no. 2013, 2015.

[5] M. Engineering, "Differences in microstructure and properties between selective laser melting and traditional ...," no. June, Springer, 2015.

[6] D. M. Rosa and D. M. Rosa, "Cellular / Dendritic Transition and Microstructure Evolution during Transient Directional Solidification of Pb-Sb Alloys" no. January, Springer US, 2008.

[7] R. L. O'Brien, "Jefferson's Welding Encyclopedia," *Am. Weld. Soc.*, vol. 18, 1997.

[8] A. C. Reardon, "Metallurgy for the Non-Metallurgist," *ASM Int.*, vol. 2, 2011.

[9] D. Wang, C. Song, Y. Yang, and Y. Bai, "Investigation of crystal growth mechanism during selective laser melting and mechanical property characterization of 316L stainless steel parts," *JMADE*, vol. 100, pp. 291–299, 2016.

[10] E. O. S. Stainlesssteel, E. O. S. Stainlesssteel, P. Set, P. Set, and P. Set, "Material data sheet EOS StainlessSteel 316L," vol. 49, no. 0, pp. 1–5, 2014.

[11] R. Casati, J. Lemke, and M. Vedani, "Journal of Materials Science & Technology Microstructure and Fracture Behavior of 316L Austenitic Stainless Steel Produced by Selective Laser Melting," *J. Mater. Sci. Technol.*, vol. 32, no. 8, pp. 738–744, 2016.

[12] S. M. Yusuf, Y. Chen, R. Boardman, S. Yang, and N. Gao, "Investigation on Porosity and Microhardness of 316L Stainless Steel Fabricated by Selective Laser Melting," pp. 1–12, Metals 2017.

[13] K. Herrmann, "Hardness Testing - Principles and Applications," *ASM Int.*, 2011.

[14] I. Lotsberg, "Fatigue Design of Marine Structures," *Cambridge Univ. Press*, 2016.

[15] G. F. Vander Voort, "ASM Handbook, Volume 09 - Metallography and Microstructures," *ASM Int.*, 2004.

[16] R. E. Chinn, "Thermal Etching" pp. 240–257, Knovel, 2015.

[17] J. Suryawanshi, K. G. Prashanth, and U. Ramamurty, "Mechanical behavior of selective laser melted 316L stainless steel," *Mater. Sci. Eng. A*, vol. 696, no. January, pp. 113–121, 2017.

[18] A. Ahmadi, R. Mirzaeifar, N. Shayesteh, A. Sadi, H. E. Karaca, and M. Elahinia, "Effect of manufacturing parameters on mechanical properties of 316L stainless steel parts fabricated by selective laser melting : A computational framework," *JMADE*, vol. 112, pp. 328–338, 2016.

Appendix 1

Recipe - AM 316L, hot mounted Ø 30 mm samples			
Struers DuroFast - Standards parameters			
Struers PolyFast - Standard parameters			
1. Rough grinding - Struers AbraPlan-20		4. Polishing - Struers AbraPol-20	
Stone	#150 (FEPA)	Disc	Struers MD-Dac
Coolant	Water	Coolant	Struers DP-Lubricant Blue
Suspension	-	Suspension	Struers DP-Suspension P - 3 µm
Time/Removal	300 µm	Time/Removal	5 minute(s)
Force	30 N/sample	Force	20 N/sample
RPM (Holder/Stone)	150/500	RPM (Holder/Disc)	150/150
2. Rough grinding - Struers AbraPol-20		5. Polishing - Struers AbraPol-20 *(1)	
Disc	Piano #220 (FEPA)	Disc	Struers MD-Nap
Coolant	Water	Coolant	Struers DP-Lubricant Blue
Suspension	-	Suspension	Struers DP-Suspension P - 1 µm
Time/Removal	1 minute(s)	Time/Removal	2 minute(s)
Force	30 N/sample	Force	20 N/sample
RPM (Holder/Disc)	150/300	RPM (Holder/Disc)	150/150
3. Fine grinding - Struers AbraPol-20		5. Polishing - Struers AbraPol-20 *(1)	
Disc	Struers MD-Largo	Disc	Struers MD-Chem
Coolant	Struers DP-Lubricant Blue	Coolant	-
Suspension	Struers DP-Suspension P - 9 µm	Suspension	Struers OP-S / OP-U
Time/Removal	4 minute(s)	Time/Removal	3 or 1 minute(s) *(2)
Force	30 N/sample	Force	15 N/sample
RPM (Holder/Disc)	150/150	RPM (Holder/Disc)	150/150
*(1) - Use either step 5 or step 6. No use of both.			
*(2) - 3 minutes for OP-S, 1 minute for OP-U			

Appendix 2

The following pictures show policed samples, in the order Z02, Z04, Z06, Z08, Z10, Z15, Z20, Z25 and Z30, there the samples porosity can be seen more clearly.

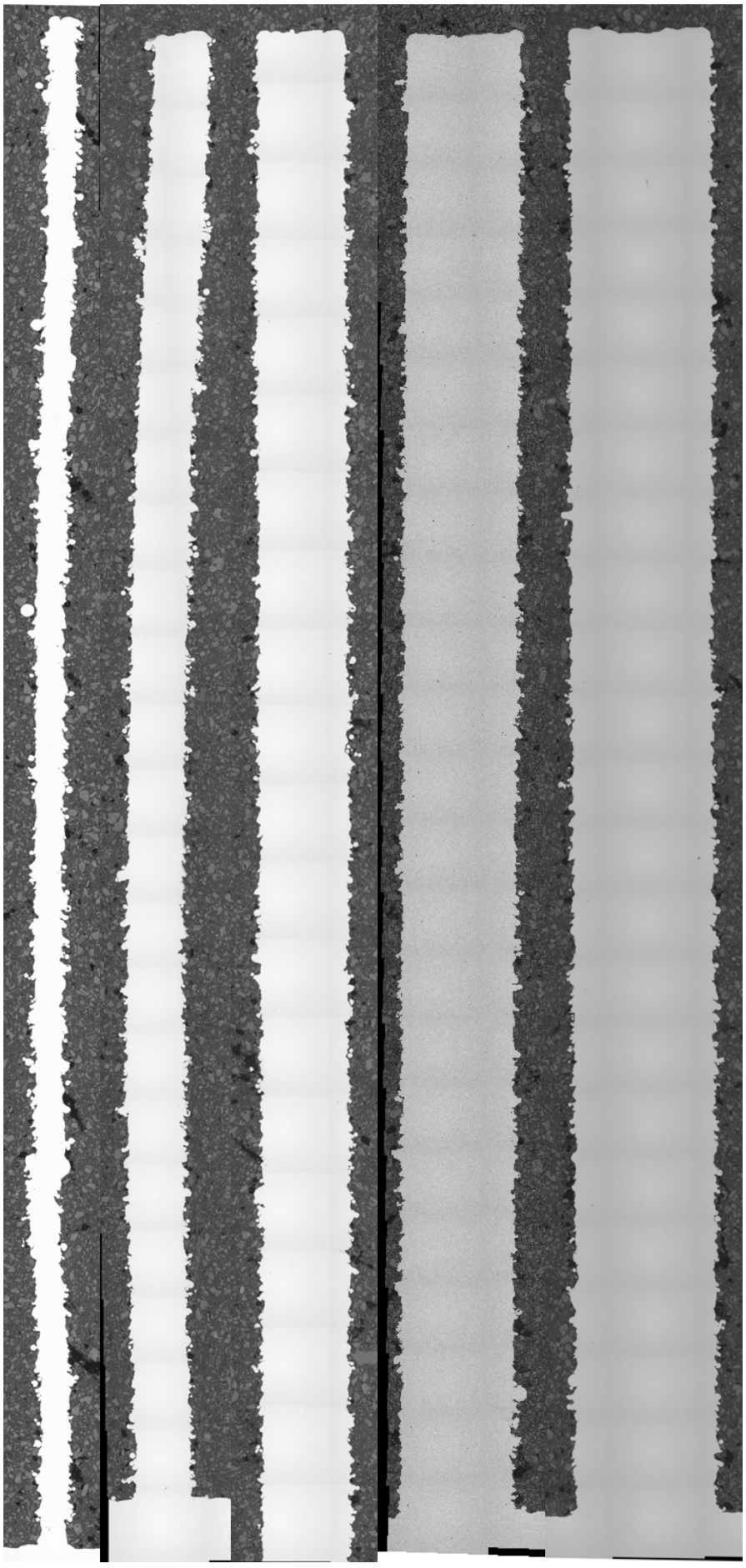

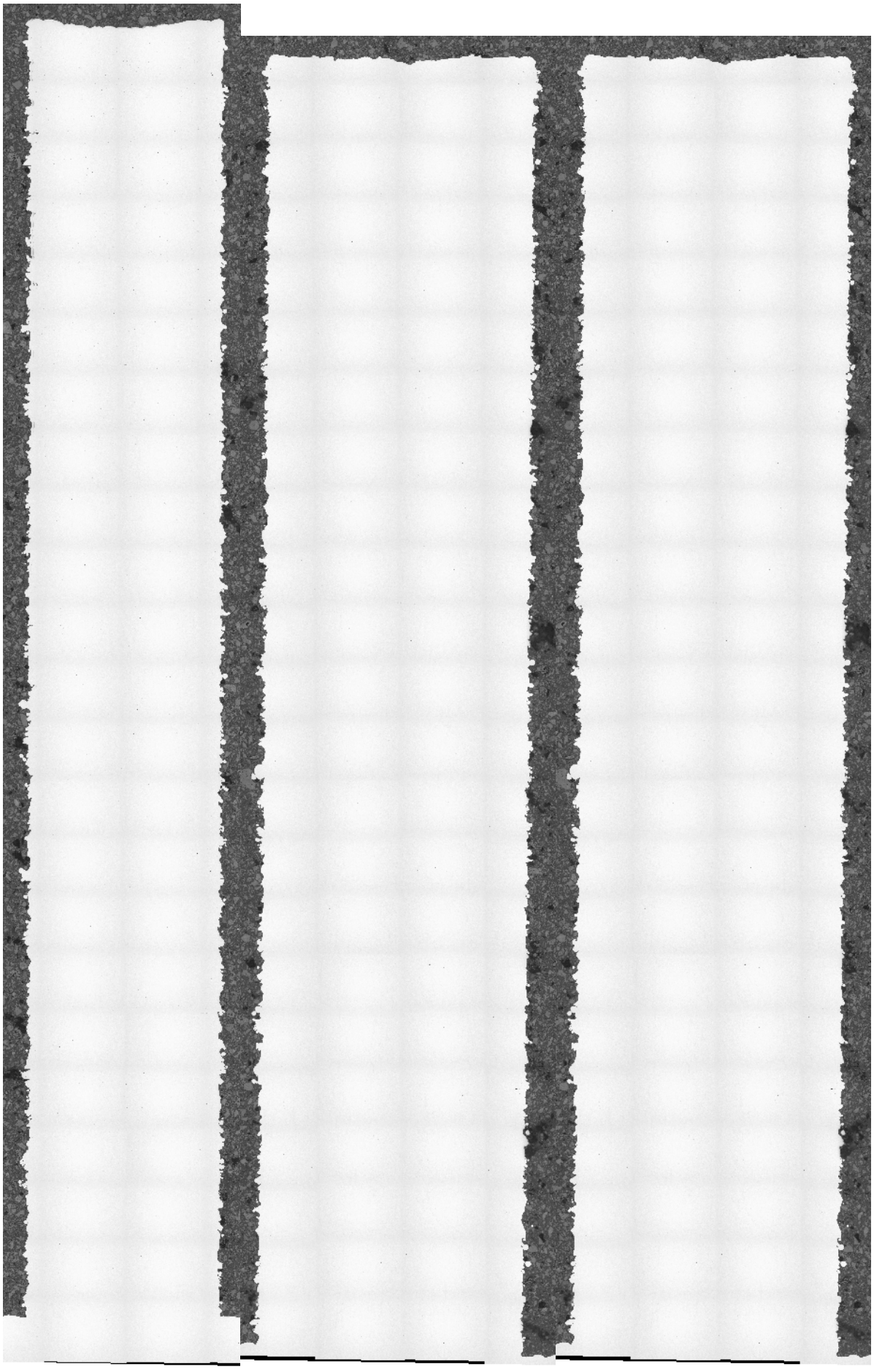

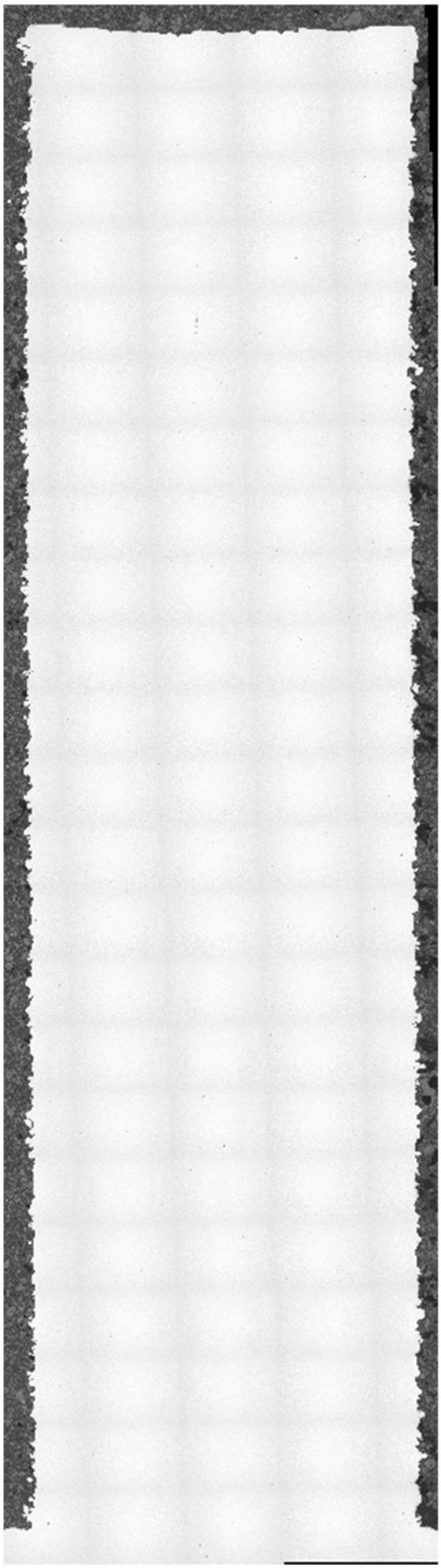

Appendix 3

Specimen	Row	Test Point	Method	Hardness	Info	Diagonal	Diagonal 1	Diagonal 2
Z02	TM	1	HV 0,1	241	OK	27.717	27.846	27.588
		2	HV 0,1	251	OK	27.2	26.985	27.416
		3	HV 0,1	235	OK	28.104	28.276	27.932
		4	HV 0,1	232	OK	28.277	28.017	28.537
		5	HV 0,1	234	OK	28.147	28.017	28.276
	MM	1	HV 0,1	241	OK	27.759	28.362	27.155
		2	HV 0,1	236	OK	28.06	27.414	28.707
		3	HV 0,1	231	OK	28.321	27.933	28.709
		4	HV 0,1	235	OK	28.061	28.017	28.106
		5	HV 0,1	249	OK	27.285	27.329	27.241
	BM	1	HV 0,1	234	OK	28.151	27.59	28.713
		2	HV 0,1	228	OK	28.494	29.052	27.936
		3	HV 0,1	241	OK	27.716	28.19	27.242
		4	HV 0,1	274	OK	25.993	26.383	25.604
		5	HV 0,1	228	OK	28.491	28.793	28.19

Appendix 4

The following pictures show etched samples, in the order Z02, Z04, Z06, Z08, Z10, Z15, Z20, Z25 and Z30, there the samples microstructure can be seen as a whole.

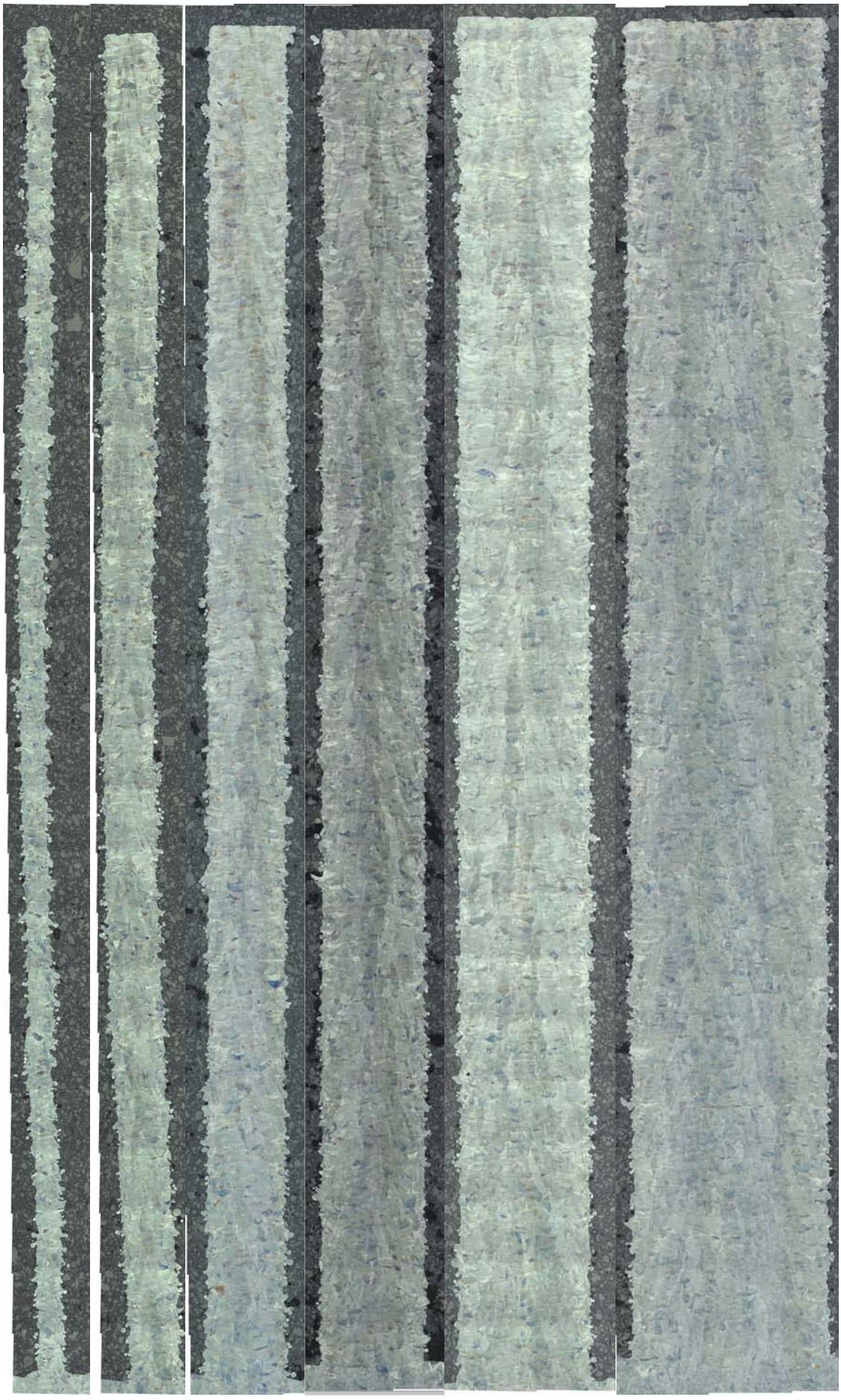

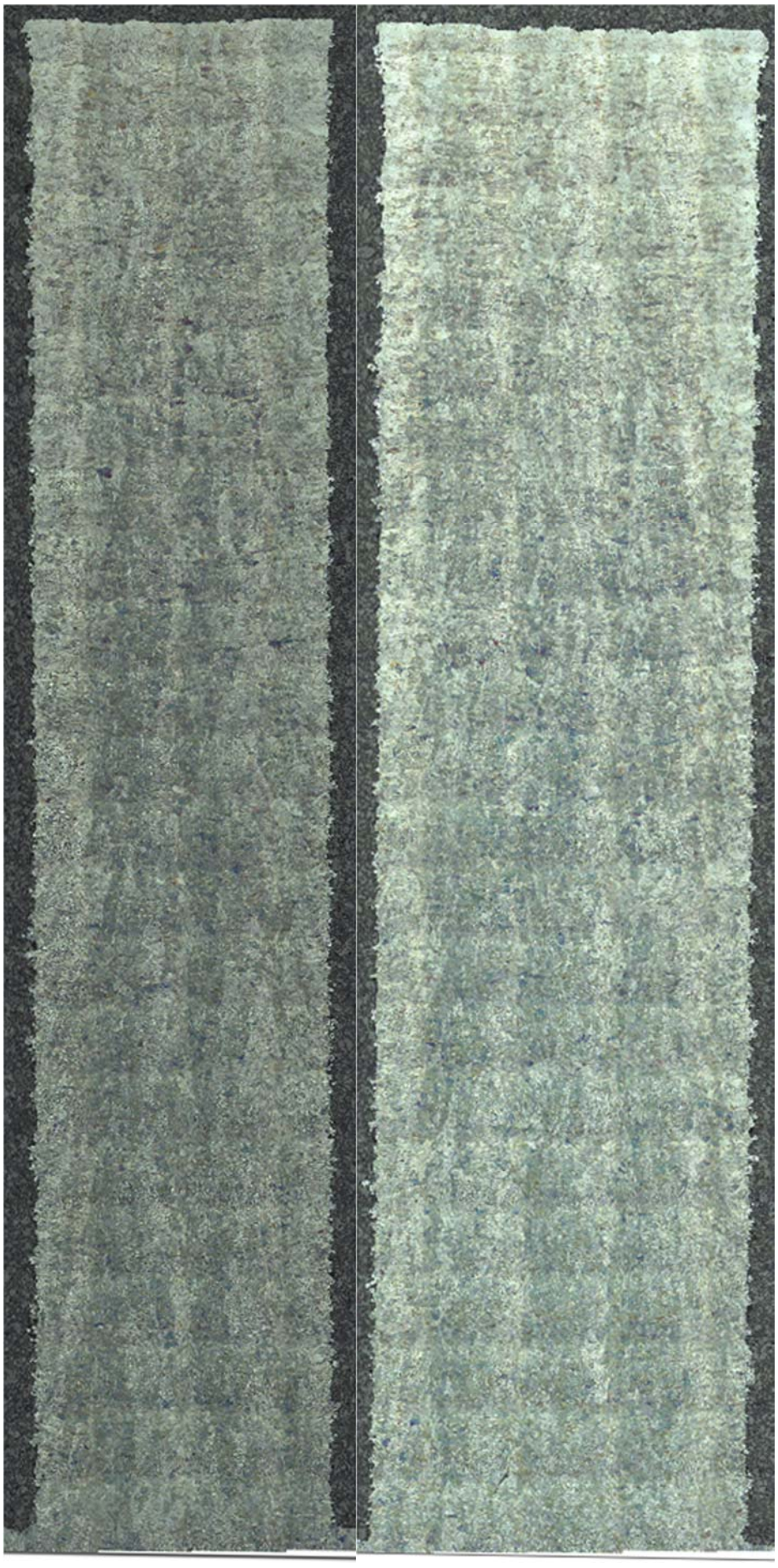

X